

RECURSIVE REDUCTION QUADRATURE FOR THE EVALUATION OF LAPLACE LAYER POTENTIALS IN THREE DIMENSIONS

SHIDONG JIANG* AND HAI ZHU†

Abstract. A high-order quadrature scheme is constructed for the evaluation of Laplace single and double layer potentials and their normal derivatives on smooth surfaces in three dimensions. The construction begins with a harmonic approximation of the density *on each patch*, which allows for a natural harmonic polynomial extension in a *volumetric neighborhood* of the patch in the ambient space. Then by the general Stokes theorem, singular and nearly singular surface integrals are reduced to line integrals preserving the singularity of the kernel, instead of the standard origin-centered 1-forms that require expensive adaptive integration. These singularity-preserving line integrals can be semi-analytically evaluated using singularity-swap quadrature. In other words, the evaluation of singular and nearly singular surface integrals is reduced to function evaluations at the vertices on the boundary of each patch. The recursive reduction quadrature largely removes adaptive integration that is needed in most existing high-order quadratures for singular and nearly singular surface integrals, resulting in exceptional performance. The scheme achieves twelve-digit accuracy uniformly for close evaluations and offers a speedup of five times or more in constructing the sparse quadrature-correction matrix compared to previous state-of-the-art quadrature schemes.

Key words. Laplace layer potential, singular integrals, nearly singular integrals, high order quadrature, integration by parts, kernel-split quadrature

AMS subject classifications. 31A08, 65D30, 65D32, 65R20

1. Introduction. We consider the evaluation of Laplace layer potentials on smooth surfaces in three dimensions. The Laplace single and double layer potentials and their normal derivatives are defined by the formulas

$$(1.1) \quad \mathcal{S}[\sigma](\mathbf{r}') = \int_S G(\mathbf{r}', \mathbf{r}) \sigma(\mathbf{r}) da(\mathbf{r}),$$

$$(1.2) \quad \mathcal{D}[\mu](\mathbf{r}') = \int_S \frac{\partial G(\mathbf{r}', \mathbf{r})}{\partial \boldsymbol{\nu}} \mu(\mathbf{r}) da(\mathbf{r}),$$

$$(1.3) \quad \mathcal{S}'[\sigma](\mathbf{r}') = \int_S \frac{\partial G(\mathbf{r}', \mathbf{r})}{\partial \boldsymbol{\nu}'} \sigma(\mathbf{r}) da(\mathbf{r}),$$

$$(1.4) \quad \mathcal{D}'[\mu](\mathbf{r}') = \int_S \frac{\partial^2 G(\mathbf{r}', \mathbf{r})}{\partial \boldsymbol{\nu}' \partial \boldsymbol{\nu}} \mu(\mathbf{r}) da(\mathbf{r}),$$

where G is the Laplace Green's function

$$(1.5) \quad G(\mathbf{r}', \mathbf{r}) = \frac{1}{4\pi|\mathbf{r}' - \mathbf{r}|}, \quad \mathbf{r}', \mathbf{r} \in \mathbb{R}^3.$$

Here, $da(\mathbf{r})$ is the surface differential at \mathbf{r} . The point \mathbf{r}' is referred to as the target point, while \mathbf{r} is the source point. The symbols $\boldsymbol{\nu}'$ and $\boldsymbol{\nu}$ represent the unit outward normal vectors at \mathbf{r}' and \mathbf{r} , respectively. We assume that the densities σ and μ are sufficiently smooth, and that the surface S is piecewise smooth and divided into a collection of patches, where each patch is sufficiently smooth and admits a high-order parameterization. Thus, the only singularity in the above integrals is induced by the Green's function or its derivatives.

*Center for Computational Mathematics, Flatiron Institute, Simons Foundation, New York, New York 10010 (sjiang@flatironinstitute.org)

†Center for Computational Mathematics, Flatiron Institute, Simons Foundation, New York, New York 10010 (hzhu@flatironinstitute.org).

When integral equation methods are applied to solve boundary value problems (BVPs) of elliptic partial differential equations, the solution is represented using layer potentials, and sometimes volume potentials as well. Imposing the boundary conditions leads to boundary integral equations (BIEs). These BIEs are discretized, and the resulting linear system is solved using either iterative solvers such as GMRES [62], accelerated by fast algorithms like the fast multipole method (FMM) [29, 30, 33, 12, 14, 23, 26, 34, 76, 78], or fast direct solvers [6, 13, 16, 24, 31, 42, 44, 43, 46, 49, 50, 51, 53, 73]. Finally, layer potentials are evaluated to obtain the solution throughout the domain. Thus, layer potentials are fundamental building blocks in fast integral equation methods: they are used in both the solve phase and the evaluation phase. Their accuracy greatly affects the accuracy of the BVP solution, and their efficiency is often a bottleneck in the solver’s overall speed.

Many engineering applications involve complex geometries where mesh generation – such as triangulation – is the initial step in discretization. In such cases, a *local quadrature* method divides the entire surface into a collection of elements with finite geometries (also referred to as chunks, panels, or patches in the literature) and then constructs quadrature nodes and weights for each element. Consequently, one only needs to consider the evaluation of Laplace layer potentials (1.1) – (1.4) when the surface S is replaced by one of these patches, denoted as P . We will primarily focus on triangular patches to avoid diverting the reader from the main ideas with technical details specific to non-triangular patches, even though our quadrature scheme essentially works for patches of *arbitrary shape*.

Depending on the distance of the target to the source patch, there are altogether four cases:

- (a) Smooth interaction: the target \mathbf{r}' is sufficiently far from the source element.
- (b) Self interaction: the target \mathbf{r}' is on the source element.
- (c) Near interaction: the target \mathbf{r}' is not on the source element, but on S and close to the source element.
- (d) Close evaluation: the target \mathbf{r}' is off-surface and close to the source element.

In the case of smooth interaction, the integrals are smooth, and high-order quadrature can be used to evaluate layer potentials in both two and three dimensions. For case (b), the integrals are weakly singular (i.e., integrable in the Riemann sense, mostly with logarithmic singularity in two dimensions or $1/r$ singularity in three dimensions for layer potentials), singular (i.e., the so-called principal value integrals), or hypersingular (i.e., the so-called Hadamard finite-part integrals). With a slight abuse of terminology, we will simply refer to case (b) as singular integrals. For cases (c) and (d), the integrals are nearly weakly singular, nearly singular, or nearly hypersingular. With a slight abuse of terminology, we will refer to these two cases as near-singular integrals. The difference between case (c) and case (d) is that the target point is associated with a parameter value in the parameter space for S in case (c), while the target point only has coordinates in the underlying physical space in case (d). Somewhat counterintuitive to those unfamiliar with integral equation methods, case (b) is actually not so hard to handle. Since the target is on the source element, various techniques can be employed to remove or cancel out the singularity in the kernels. Case (d) proves to be the most challenging because the target lies in the ambient space and lacks an associated parameter value, rendering many singularity subtraction or removal techniques inapplicable.

Over the past fifty years or so, numerous researchers have tackled this important problem. In [19, 27, 28, 70, 71, 72], high-order global quadratures have been developed for surfaces homeomorphic to the sphere or torus. In [20] and subsequently [10, 11],

polar coordinates centered at the given target point are used to eliminate the $1/r$ singularity for self interactions. In [7, 8], *generalized Gaussian quadrature* (GGQ) [9, 48, 75] is applied along each radial direction in polar coordinates to achieve better efficiency and accuracy, capable of handling triangles with aspect ratio as high as a million. For cases (c) and (d), a popular approach is to evaluate layer potentials for targets sufficiently away from the surface using oversampled smooth quadrature rule, then apply interpolation/extrapolation to evaluate the layer potential at the given target point. This includes the QBX (*quadrature by expansions*) [22, 45, 59, 64, 68, 69], its descendants [17, 54, 65], and methods in [4, 5]. Recently, there are also quadratures based on the harmonic density interpolation [56], planewave density interpolation [57], and adaptive integration [32] that combines the FMM and careful precomputed tables.

In this paper, we introduce a unified quadrature scheme that handles self and near interactions, as well as close evaluations, eliminating the need for adaptive integration. For the Laplace double layer potential (DLP), we first approximate the density σ on P in *quaternion algebra* such that the resulting approximation has a *natural harmonic polynomial extension*. The harmonic polynomial extension is valid in the whole ambient space, but only needed in a *volumetric neighborhood* of P . Such density approximation enables the application of the *general Stokes theorem* without any further approximation in exact arithmetics and reduces singular and nearly singular integrals on the surface patch P to line integrals on the boundary of P . In other words, the scheme approximates the density in such a way that one may apply the integration by parts formula to analytically reduce surface integrals to line integrals on the boundary of each surface patch. This differs from all prior approaches except the work in [79, 80]. We then derive new expressions of these line integrals such that they preserve the singularity and translation invariance of the kernels in the original surface integrals. The advantage of doing this is that we can apply the singularity-swap quadrature [1] to evaluate these nearly singular line integrals analytically by recurrence. To be more precise, the new line integrals can be evaluated via another step of integration by parts, this time by extending the parameter into the complex plane rather than using the general Stokes theorem. Hence the *recursive reduction quadrature* (RRQ).

We describe in detail the improvements made in RRQ over the work in [79, 80] in [subsection 3.1](#). Here, we summarize the novel features that make it more elegant, accurate, and efficient than other existing methods.

- (1) Unlike the popular Duffy quadrature used in boundary element methods and its aforementioned descendants, which are used only for self-interactions, RRQ unifies the treatment of self and near interactions, as well as close evaluations.
- (2) Unlike other existing methods that evaluate the original surface integrals directly using some kind of adaptive integration, oversampling, target interpolation or extrapolation, RRQ reduces surface integrals via integration-by-parts twice, achieving full reduction from surface integrals to function evaluations at the vertices of the surface elements.
- (3) RRQ further divides target points into two groups. The first group consists of points close to the surface but sufficiently away from the edges of the surface element, where much less computational effort is needed to evaluate the line integrals. The second group includes points close to the edges of the surface element, where the singularity-swap quadrature requires only a mild increase

in computational effort. Thus, RRQ reduces the list of targets that require significant computational effort from a neighborhood of the entire surface element to the neighborhood of its boundary.

- (4) Unlike some existing methods that rely on asymptotics or low-order density approximations, RRQ can achieve much higher convergence order and accuracy.

Combining all these features, RRQ achieves high efficiency and robustness and can be constructed to have arbitrarily high order. It attains twelve-digit accuracy uniformly for close evaluations and provides a speedup of fivefold or more over previous state-of-the-art quadrature methods.

The outline of the paper is as follows. In [section 2](#), we collect and review the analytical apparatus used in the rest of the paper. In [section 3](#), we present the main theoretical results. In [section 4](#), we discuss the algorithmic steps in the scheme and analyse the cost of each step. Numerical examples are shown in [section 5](#). Finally, [section 6](#) contains some further remarks on future extensions of the work.

2. Mathematical apparatus. In this section, we collect some results to be used in later sections, including quaternion algebra, exterior derivatives, differential forms, general Stokes theorem, harmonic polynomials, singularity-swap quadrature, and key results from [\[79, 80\]](#). We would like to remark here that even though it might be possible to write the entire paper using vector calculus, we choose to use quaternion algebra and differential forms due to the following reasons. First, quaternion algebra greatly simplifies many equations. Second, exterior derivatives and differential forms are standard tools for the general Stokes theorem. The use of differential forms, which employ Cartesian coordinates in the ambient space, also makes it easy to understand why close evaluation can be treated the same way as near interactions. Nevertheless, the paper remains mostly self-contained, and the use of quaternion algebra and differential forms is minimized to ensure it is easily accessible to readers.

2.1. Quaternion algebra. The quaternion algebra, as pointed out in [\[61\]](#), is the even part of the Clifford algebra. For a quaternion $f = f_0 + f_1\mathbf{i} + f_2\mathbf{j} + f_3\mathbf{k}$, we also write it as $f = (f_0, \mathbf{f})$, where f_0 and \mathbf{f} are the scalar and vector parts of the quaternion f , respectively. Here, we identify three imaginary basis vectors \mathbf{i} , \mathbf{j} , \mathbf{k} in the quaternion algebra with three basis vectors in \mathbb{R}^3 . The product of two quaternions, $f = (f_0, \mathbf{f})$ and $g = (g_0, \mathbf{g})$, can then be expressed using the dot and cross products of vectors as follows:

$$(2.1) \quad fg = (f_0g_0 - \mathbf{f} \cdot \mathbf{g}, f_0\mathbf{g} + g_0\mathbf{f} + \mathbf{f} \times \mathbf{g}),$$

where \cdot denotes the vector dot product, and \times denotes the cross product. The quaternion (and the Clifford) algebra is associative, but non-commutative. That is, if f , g , and h are three quaternions, then $(fg)h = f(gh)$, but $fg \neq gf$ in general. The conjugate of a quaternion f is denoted as $\bar{f} = (f_0, -\mathbf{f})$, and the length of f is denoted as $|f| = \sqrt{f\bar{f}} = \sqrt{f_0^2 + |\mathbf{f}|^2}$. It is easy to check that $f_0g = (f_0, \mathbf{0})g = g(f_0, \mathbf{0})$. Thus, we identify a scalar f_0 with the quaternion $(f_0, \mathbf{0})$.

2.2. Differential forms and Stokes theorem. The general Stokes theorem on differential forms is stated as [\[18\]](#)

$$(2.2) \quad \int_{\partial D} \omega = \int_D d\omega,$$

where ω is a k -form, d is the exterior derivative, and ∂D is the boundary of D . A differential form ω is closed if $d\omega = 0$, and exact if $\omega = d\alpha$ for some other differential form α . Because $d^2 = 0$, every exact form is closed. The Poincaré lemma [18] states that every closed form is exact when the domain is contractible. For the rest of the paper, we always assume that the surface S is divided into a collection of contractible patches such that the Poincaré lemma is valid on every patch P . It is clear that the assumption holds for all reasonable discretizations encountered in practice. Straightforward calculation shows that the area differential $\boldsymbol{\nu}(\mathbf{r})da(\mathbf{r})$ can be written in terms of the differential 2-forms as follows:

$$(2.3) \quad \boldsymbol{\nu}(\mathbf{r})da(\mathbf{r}) = dy \wedge dz \mathbf{i} + dz \wedge dx \mathbf{j} + dx \wedge dy \mathbf{k},$$

where $\mathbf{r} = (x, y, z)$. Thus, a surface integral of a vector field in three dimensions is equivalent to the integral of differential 2-forms, expressed as follows:

$$(2.4) \quad \int_S \mathbf{f}(\mathbf{r}) \cdot \boldsymbol{\nu}(\mathbf{r})da(\mathbf{r}) = \int_S f_1 dy \wedge dz + f_2 dz \wedge dx + f_3 dx \wedge dy.$$

The following lemma summarizes the analytical results required to convert surface integrals over a patch P to line integrals along its boundary ∂P .

LEMMA 2.1. *Suppose that P is a contractible surface element in \mathbb{R}^3 and that f is a real-valued function defined in a neighborhood of P in \mathbb{R}^3 . Then the differential 2-form $\alpha = \mathbf{f}(\mathbf{r}) \cdot \boldsymbol{\nu}(\mathbf{r})da(\mathbf{r})$ is closed if and only if $\nabla \cdot \mathbf{f} = 0$. Furthermore, if α is closed, then for any fixed point $\mathbf{p} \in \mathbb{R}^3$ the 1-form β defined by the formula*

$$(2.5) \quad \beta = \left(- \int_0^1 t(\mathbf{r} - \mathbf{p}) \times \mathbf{f}(\mathbf{p} + t(\mathbf{r} - \mathbf{p})) dt \right) \cdot d\mathbf{r}$$

satisfies the equation

$$(2.6) \quad d\beta = \alpha,$$

and thus

$$(2.7) \quad \int_P \alpha = \int_{\partial P} \beta.$$

In other words, the surface integral $\int_P \alpha$ is reduced to line integrals on its boundary, i.e., the integral of a 1-form with the 1-form explicitly given by (2.5).

Proof. By (2.4), we have

$$(2.8) \quad d\alpha = \nabla \cdot \mathbf{f} dx \wedge dy \wedge dz.$$

And the first statement follows. In order to prove the second statement, a straightforward calculation that is almost identical to that of Lemma 3.2 in [79, 80] shows that $d\beta = \alpha$ for any fixed \mathbf{p} . Then the second statement follows from the general Stokes theorem (2.2). \square

2.3. Harmonic polynomials. The associated Legendre polynomials P_l^m are defined by the formula [55]

$$(2.9) \quad P_l^m(x) = \frac{1}{2^l l!} (1-x^2)^{m/2} \frac{d^{l+m}}{dx^{l+m}} (x^2-1)^l.$$

Here, l is a nonnegative integer and $-l \leq m \leq l$. For a given x , all values of $P_l^m(x)$ for $l = 0, \dots, p$ and $m = 0, \dots, l$ can be calculated via the following recurrence formulas:

$$(2.10) \quad \begin{aligned} P_0^0(x) &= 1, \\ P_{l+1}^{l+1}(x) &= -(2l+1)\sqrt{1-x^2}P_l^l(x), \\ P_{l+1}^l(x) &= (2l+1)xP_l^l(x), \\ (l-m+1)P_{l+1}^m(x) &= (2l+1)xP_l^m(x) - (l+m)P_{l-1}^m(x). \end{aligned}$$

The spherical harmonic polynomials Y_l^m are defined by the formula

$$(2.11) \quad Y_l^m(\theta, \phi) = \sqrt{2l+1} \sqrt{\frac{(l-m)!}{(l+m)!}} P_l^m(\cos(\theta)) e^{im\phi},$$

where we have dropped the normalization factor $\frac{1}{\sqrt{4\pi}}$ and the Condon-Shortley phase $(-1)^m$.

The regular solid harmonic polynomials R_l^m are defined by the formula

$$(2.12) \quad R_l^m(\mathbf{r}) = \frac{1}{\sqrt{2l+1}} r^l Y_l^m(\theta, \phi),$$

where (r, θ, ϕ) are the spherical polar coordinates of \mathbf{r} . Note that $R_l^m(\mathbf{r})$ is a homogeneous polynomial of degree l in its Cartesian coordinates (x, y, z) .

The translation of the regular solid harmonic is given by the formula [14, 29, 30]

$$(2.13) \quad R_l^m(\mathbf{r}) = \sum_{j=0}^l \sum_{k=-j}^j R_j^k(\mathbf{r} - \mathbf{r}') R_{l-j}^{m-k}(\mathbf{r}') T_{jk,lm},$$

where the coefficient $T_{jk,lm}$ is given by the formula

$$(2.14) \quad T_{jk,lm} = \binom{l+m}{j+k}^{1/2} \binom{l-m}{j-k}^{1/2}.$$

Harmonic functions can be approximated by a harmonic polynomial expansion of the p th order

$$\sum_{l=0}^p \sum_{m=-l}^l C_l^m R_l^m(\mathbf{r}).$$

Note that this is exactly the so-called local expansion in the fast multipole method [14], and it can be evaluated via the recurrence (2.10) efficiently. The translation of local expansions can be carried out using (2.13) and (2.14) as follows:

$$(2.15) \quad \sum_{l=0}^p \sum_{m=-l}^l C_l^m R_l^m(\mathbf{r}) = \sum_{j=0}^p \sum_{k=-j}^j D_j^k R_j^k(\mathbf{r} - \mathbf{r}'),$$

where

$$(2.16) \quad D_j^k = \sum_{l=j}^p \sum_{m=-l}^l T_{jk,lm} R_{l-j}^{m-k}(\mathbf{r}') C_l^m.$$

REMARK 2.2. *The direct application of (2.15)–(2.16) requires $O(p^4)$ work. In [34], the translation is carried out by rotation of $\mathbf{r} - \mathbf{r}'$ to z -axis, translating along the z -axis, and another rotation back to the original coordinate system. The total cost of the scheme in [34] is $O(p^3)$.*

2.4. Singularity-swap quadrature. In [1], a singularity-swap quadrature is proposed to evaluate nearly singular line integrals of the form

$$(2.17) \quad I(\mathbf{r}') = \int_{-1}^1 \frac{f(t)}{|\mathbf{r}(t) - \mathbf{r}'|^m} dt, \quad m = 1, 3, \dots,$$

where f is a smooth function and $\mathbf{r}(t) = (x(t), y(t), z(t))$ is the vector function with the real-valued parameter t defining a space curve Γ in three dimensions. The key observation in [1] is to find a complex number t_0 such that

$$(2.18) \quad (x(t_0) - x')^2 + (y(t_0) - y')^2 + (z(t_0) - z')^2 = 0.$$

That is, we extend the real-valued argument of the function $\mathbf{r}(t)$ to the complex plane and then find a complex number t_0 such that (2.18) holds for the given target point $\mathbf{r}' = (x', y', z') \in \mathbb{R}^3$. Then (2.17) can be rewritten as

$$(2.19) \quad I(\mathbf{r}') = \int_{-1}^1 \frac{F(t)}{((t - t_0)(t - \bar{t}_0))^{m/2}} dt,$$

where

$$(2.20) \quad F(t) = f(t) \frac{|t - t_0|^m}{|\mathbf{r}(t) - \mathbf{r}'|^m}.$$

Since both $|t - t_0|^2 = (t - t_0)(t - \bar{t}_0)$ and $|\mathbf{r}(t) - \mathbf{r}'|^2 = (x(t) - x')^2 + (y(t) - y')^2 + (z(t) - z')^2$ have the same roots t_0 and \bar{t}_0 in the complex plane, $F(t)$ is again a smooth function of t for $t \in [-1, 1]$. And the construction of the quadrature is completed by the observation that integrals of the form

$$\int_{-1}^1 \frac{t^i}{((t - t_0)(t - \bar{t}_0))^{m/2}} dt, \quad i = 0, 1, 2, \dots$$

can be evaluated analytically via a recurrence relation.

2.5. Summary of main analytic results in [79, 80]. At the heart of the quadrature scheme in [79, 80] lies the *local quaternion harmonic approximation* of the density on each patch P . Consider the Laplace double layer potential (DLP) defined by (1.2) with the whole surface S replaced by a contractable patch P . Suppose that $H^{(l,m)}(\mathbf{r})$ are harmonic polynomials. Then the following quaternion 2-forms [80, Corollary 3.4]

$$(2.21) \quad \alpha^{(l,m)}(\mathbf{r}', \mathbf{r}) = (0, \nabla G(\mathbf{r}', \mathbf{r}))(0, \boldsymbol{\nu}(\mathbf{r}))(0, \nabla H^{(l,m)}(\mathbf{r})) da(\mathbf{r})$$

are closed and exact. Thus, there exist 1-forms $\beta^{(l,m)}$ such that

$$(2.22) \quad d\beta^{(l,m)}(\mathbf{r}', \mathbf{r}) = \alpha^{(l,m)}(\mathbf{r}', \mathbf{r}).$$

By direct calculation, we have

$$(2.23) \quad (0, \nabla G(\mathbf{r}', \mathbf{r}))(0, \boldsymbol{\nu}(\mathbf{r}))(\mu(\mathbf{r}), \mathbf{0}) = (-[\nabla G(\mathbf{r}', \mathbf{r}) \cdot \boldsymbol{\nu}(\mathbf{r})] \mu(\mathbf{r}), [\nabla G(\mathbf{r}', \mathbf{r}) \times \boldsymbol{\nu}(\mathbf{r})] \mu(\mathbf{r})),$$

and the following lemma.

LEMMA 2.3. *Suppose that the density μ of the Laplace double layer potential is approximated via the following p th order quaternion harmonic approximation on a contractable patch P [80, Eq. (21)]*

$$(2.24) \quad (\mu(\mathbf{r}), \mathbf{0}) \approx \sum_{l=1}^p \sum_{m=1}^l (0, \nabla H^{(l,m)}(\mathbf{r})) c^{(l,m)}, \quad \mathbf{r} \in P,$$

where $c^{(l,m)}$ are quaternion coefficients of the form

$$(2.25) \quad c^{(l,m)} = c_0^{(l,m)} + c_1^{(l,m)} \mathbf{i} + c_2^{(l,m)} \mathbf{j} + c_3^{(l,m)} \mathbf{k}.$$

Suppose further that the quaternion Q is defined by the formula

$$(2.26) \quad Q[\mu](\mathbf{r}') = \int_P (0, \nabla G(\mathbf{r}', \mathbf{r})) (0, \boldsymbol{\nu}(\mathbf{r})) (\mu(\mathbf{r}), \mathbf{0}) da(\mathbf{r}).$$

Then

$$(2.27) \quad \mathcal{D}[\mu](\mathbf{r}') = -Q_0[\mu](\mathbf{r}'),$$

i.e., the double layer potential is the negative scalar part of the quaternion Q . Thus,

$$(2.28) \quad \begin{aligned} \mathcal{D}[\mu](\mathbf{r}') &= -Q_0[\mu](\mathbf{r}') \\ &\approx - \sum_{l,m} \int_P \left[\alpha^{(l,m)}(\mathbf{r}', \mathbf{r}) c^{(l,m)} \right]_0 \\ &= - \sum_{l,m} \int_{\partial P} \left[\beta^{(l,m)}(\mathbf{r}', \mathbf{r}) c^{(l,m)} \right]_0, \end{aligned}$$

where $[\cdot]_0$ denotes the scalar part of the quaternion.

Lemma 2.3 shows that the evaluation of the Laplace double layer potential on P is reduced to that of the quaternion 1-forms (line integrals) on ∂P .

3. Main results.

3.1. Summary of improvements made over the work in [79, 80]. The work in [79, 80] is quite original and offers a fresh starting point for the evaluation of layer potentials in three dimensions. However, it is incomplete and has several major drawbacks. First, [79, 80] provides explicit expressions of the harmonic basis functions only up to order seven. A rigorous proof that those functions form a complete basis is missing. It is also unclear how to construct such basis functions for arbitrary order. Second, the kernels of line integrals in [79, 80] have weaker but more complicated singularity. Indeed, the construction of line integrals in [79, 80] depends on the choice of the origin, and as a result the singularity of the kernels depends not only on the difference vector of the target and source points, but also on the absolute coordinates of the target and source points. In other words, the translation invariance of the kernel is lost. This leads to expensive adaptive integration to resolve the near-singularity in the kernel when the target point is close to the boundary curves. Consequently, the efficiency gains achieved by the reduction to line integrals are significantly eroded, resulting in unsatisfactory performance. Third, in [79, 80] the Laplace single layer potential (SLP) is converted to the Laplace double layer potential with a *target-dependent density*. While this method works, it is somewhat *ad hoc* and requires

three quaternion DLP density approximations, resulting in significant computational slowdown.

Here, we fill in the missing pieces and present solutions to overcome these drawbacks, which significantly improves performance and reliability. First, we show that a set of complete and linearly independent basis functions can be chosen for the quaternion harmonic polynomial approximation of the density for flat triangular patches for any given order ([Theorem 3.1](#)). This puts the construction of the quadrature scheme in a solid footing and extends the scheme to arbitrary high order. Second, we develop a new integration-by-parts formula for the Laplace single layer potential ([Theorem 3.12](#)), resulting in a threefold speedup. Third, in order to remove the adaptive integration from the scheme, we switch to the target-centered 1-forms ([Theorem 3.14](#) and [Theorem 3.16](#)) (i.e., line integrals) from the origin-centered 1-forms in [79, 80]. These target-centered 1-forms preserve the singularity of the kernel, enabling the use of singularity-swap quadrature [1] to evaluate these nearly singular line integrals analytically by recurrence. To be more precise, the 1-forms are further reduced to 0-forms through another application of integration by parts, achieved by extending the parameter into the complex plane rather than using the general Stokes theorem. Finally, we apply the fast translation [34] of local expansions in the FMM and carefully separate the source-dependent steps from the target-dependent steps in the whole scheme to improve its efficiency ([section 4](#)).

3.2. Choice of basis functions for the p th order harmonic approximation. We now discuss how to choose basis functions $H^{(l,m)}$ in the quaternion harmonic approximation (2.24) for the p th order scheme. For standard polynomial approximation on a flat triangle on the xy -plane, one may use $x^i y^j$ with $0 \leq i + j \leq p - 1$ or their suitable linear combinations (such as the Koornwinder polynomials [47]) as the basis functions for the p th order scheme. It is not clear how one should choose harmonic polynomials $H^{(l,m)}$ ($1 \leq m \leq l \leq p$) in (2.24) such that their gradients span the proper subspace for the desired convergence order. In [79, 80], the authors explicitly describe basis functions $H^{(l,m)}$ for $p \leq 7$ and observe that empirically it works. Below we show how to select such basis functions $H^{(l,m)}$ ($1 \leq m \leq l \leq p$) for any given order p for flat triangles on the xy -plane.

We start from the standard solid harmonic polynomials $R_l^m(\mathbf{r}) = R_l^m(x, y, z)$ in (2.12). In order to obtain real harmonic polynomials, we consider

$$(3.1) \quad \tilde{H}^{(l,m)}(x, y, z) = \frac{i}{\sqrt{2}} \left(-(-1)^m R_l^m(x, y, z) + R_l^{-m}(x, y, z) \right).$$

In Cartesian coordinates, we have [55]

$$(3.2) \quad \tilde{H}^{(l,m)}(x, y, z) = \left[\frac{2(l-m)!}{(l+m)!} \right]^{1/2} \Pi_l^m(z, r) B_m(x, y),$$

where

$$(3.3) \quad B_m(x, y) = \frac{1}{2i} [(x + iy)^m - (x - iy)^m],$$

and

$$(3.4) \quad \Pi_l^m(z, r) = r^{l-m} \frac{d^m P_l(u)}{du^m} = \sum_{k=0}^{\lfloor (l-m)/2 \rfloor} \gamma_{lk}^{(m)} r^{2k} z^{l-2k-m},$$

with P_l the Legendre polynomial of degree l , $u = \cos \theta = \frac{z}{r}$, and

$$(3.5) \quad \gamma_{lk}^{(m)} = (-1)^k 2^{-l} \binom{l}{k} \binom{2l-2k}{l} \frac{(l-2k)!}{(l-2k-m)!}.$$

The following theorem provides one way of constructing proper basis functions $H^{(l,m)}$ ($1 \leq m \leq l \leq p$) for the quaternion harmonic approximation (2.24).

THEOREM 3.1. *Let*

$$(3.6) \quad H^{(l,m)}(x, y, z) := \tilde{H}^{(l,m)}(y, z, x) = \left[\frac{2(l-m)!}{(l+m)!} \right]^{1/2} \Pi_l^m(x, r) B_m(y, z).$$

Then on the xy -plane,

$$(3.7) \quad \nabla H^{(l,m)}(x, y, 0) = (0, 0, \frac{\partial H^{(l,m)}(x, y, 0)}{\partial z}) := (0, 0, F^{(l,m)}(x, y)),$$

and for any $p \geq 1$,

$$(3.8) \quad \text{span}\{F^{(l,m)} | l = 1, \dots, p, m = 1, \dots, l\} = \text{span}\{x^i y^j | 0 \leq i + j \leq p - 1\}.$$

In other words, $F^{(l,m)}$ ($l = 1, \dots, p, m = 1, \dots, l$) form a complete and linearly independent basis for the p th order polynomial approximation on the xy -plane.

Theorem 3.1 is proved by induction and direct calculations. We break the proof into the following lemmas.

LEMMA 3.2.

$$(3.9) \quad B_m(y, z) = z C_{m-1}(y, z),$$

where $C_{m-1}(y, z)$ is a polynomial in y and z of degree at most $m - 1$.

Proof. By the definition of B_m , we have

$$(3.10) \quad B_m(y, z) = \frac{1}{2i} [(y + iz)^m - (y - iz)^m].$$

Thus, $B_m(y, z)$ is a polynomial in y and z of degree at most m . Furthermore, it is clear that $B_m(y, 0) = 0$. That is, $z = 0$ is a root of $B_m(y, \cdot)$ as a function of z . Therefore, z can be factored out, which leads to (3.9). \square

LEMMA 3.3.

$$(3.11) \quad \frac{\partial H^{(l,m)}(x, y, 0)}{\partial x} = 0, \quad \frac{\partial H^{(l,m)}(x, y, 0)}{\partial y} = 0.$$

Proof. By direct calculations, we have

$$(3.12) \quad \begin{aligned} \frac{\partial H^{(l,m)}(x, y, z)}{\partial x} &= B_m(y, z) \frac{\partial \Pi_l^m(x, y, z)}{\partial x}, \\ \frac{\partial H^{(l,m)}(x, y, z)}{\partial y} &= B_m(y, z) \frac{\partial \Pi_l^m(x, y, z)}{\partial y} + z \frac{\partial C_{m-1}(y, z)}{\partial y}. \end{aligned}$$

And the lemma follows from $B_m(y, 0) = 0$. \square

Direct calculations also lead to the following lemmas.

LEMMA 3.4.

$$(3.13) \quad \Pi_l^m(x, r|_{z=0}) := D_l^m(x, y) = \sum_{k=0}^{\lfloor (l-m)/2 \rfloor} \gamma_{lk}^{(m)} (x^2 + y^2)^k x^{l-2k-m}.$$

In particular,

$$(3.14) \quad D_l^l(x, y) = \gamma_{l0}^{(l)}, \quad D_l^{l-1}(x, y) = \gamma_{l0}^{(l-1)} x.$$

LEMMA 3.5.

$$(3.15) \quad \frac{\partial H^{(l,m)}(x, y, 0)}{\partial z} = F^{(l,m)}(x, y) = D_l^m(x, y) C_{m-1}(y, 0).$$

LEMMA 3.6.

$$(3.16) \quad C_{m-1}(y, 0) = my^{m-1}, \quad m = 1, 2, \dots$$

LEMMA 3.7. For $l \geq 1$, $F^{(l,m)}$ is a homogeneous polynomial of degree $l-1$ for all $m = 1, \dots, l$. Furthermore for any $0 \leq k \leq l-1$,

$$(3.17) \quad \text{span}\{F^{(l,m)}(x, y) | m = l, l-1, \dots, l-k\} = \text{span}\{y^{l-1}, xy^{l-2}, \dots, x^k y^{l-k-1}\}.$$

Proof. We prove it by induction. First, the statement is true for $k=0$ since

$$(3.18) \quad F^{(l,l)}(x, y) = D_l^l(x, y) C_{l-1}(y, 0) = l\gamma_{l0}^{(l)} y^{l-1}.$$

Suppose that the statement is true for all $k \leq n$. Then for $k = n+1$, we have

$$(3.19) \quad \text{span}\{F^{(l,m)}(x, y) | m = l, \dots, l-n-1\} = \text{span}\{y^{l-1}, \dots, x^n y^{l-n-1}, F^{(l, l-n-1)}(x, y)\}.$$

Combining (3.13)–(3.16), we have

$$(3.20) \quad \begin{aligned} F^{(l, l-n-1)}(x, y) &= (l-n-1)y^{l-n-2} \sum_{k=0}^{\lfloor (n+1)/2 \rfloor} \gamma_{lk}^{(l-n-1)} (x^2 + y^2)^k x^{n+1-2k} \\ &= c_0 y^{l-n-2} x^{n+1} + c_1 y^{l-n} x^{n-1} + \dots \end{aligned}$$

It is easy to see that all lower order terms in (3.20) already appear in the first n terms of the right side of (3.19). Thus,

$$(3.21) \quad \text{span}\{y^{l-1}, \dots, x^n y^{l-n-1}, F^{(l, l-n-1)}(x, y)\} = \text{span}\{y^{l-1}, \dots, x^n y^{l-n-1}, x^{n+1} y^{l-n-2}\}. \blacksquare$$

And the lemma follows. \square

It is clear that [Theorem 3.1](#) follows from [Lemma 3.7](#).

We now choose a set of collocation points $\mathbf{r}^{(i,j)}$ ($0 \leq i+j \leq p-1$) on the triangular patch P . In the community of integral equation methods, popular choices include Vioreanu-Rokhlin nodes [67] and Xiao-Gimbutas nodes [74], with the latter having associated quadrature close to the Gaussian quadrature on a triangle. The quaternion coefficients $c^{(l,m)}$ in (2.24) are then obtained by solving the following linear system, which imposes equality at these points in (2.24):

$$(3.22) \quad \sum_{l=1}^p \sum_{m=1}^l (0, \nabla H^{(l,m)}(\mathbf{r}^{(i,j)})) c^{(l,m)} = (\mu(\mathbf{r}^{(i,j)}), \mathbf{0}), \quad 0 \leq i+j \leq p-1.$$

Writing out explicitly, (3.22) is equivalent to the following equations with only the usual vector calculus involved:

$$(3.23) \quad \begin{aligned} & - \sum_{l,m} \nabla H^{(l,m)}(\mathbf{r}^{(i,j)}) \cdot \mathbf{c}^{(l,m)} = \mu(\mathbf{r}^{(i,j)}), \\ & \sum_{l,m} c_0^{(l,m)} \nabla H^{(l,m)}(\mathbf{r}^{(i,j)}) + \nabla H^{(l,m)}(\mathbf{r}^{(i,j)}) \times \mathbf{c}^{(l,m)} = \mathbf{0}. \end{aligned}$$

Let $\nabla H = (F_1, F_2, F_3)$. Then in block matrix form, we have

$$(3.24) \quad \begin{pmatrix} 0 & -F_1 & -F_2 & -F_3 \\ F_1 & 0 & -F_3 & F_2 \\ F_2 & F_3 & 0 & -F_1 \\ F_3 & -F_2 & F_1 & 0 \end{pmatrix} \begin{pmatrix} c_0 \\ c_1 \\ c_2 \\ c_3 \end{pmatrix} = \begin{pmatrix} \mu \\ 0 \\ 0 \\ 0 \end{pmatrix},$$

where the length of c_k ($k = 0, 1, 2, 3$) is n_p with $n_p = \frac{p(p+1)}{2}$, the size of each block is $n_p \times n_p$, and the size of the full linear system is $4n_p \times 4n_p$.

REMARK 3.8. *Theorem 3.1 shows that when the patch is flat and lie in the xy -plane, the harmonic basis functions constructed in (3.6) lead to $(F_1, F_2, F_3) = (0, 0, F_3)$, and that F_3 is invertible for a set of collocation points $\{\mathbf{r}^{(i,j)} | 0 \leq i + j \leq p - 1\}$ if and only if the standard p th order monomial basis $\{x^i y^j | 0 \leq i + j \leq p - 1\}$ form linearly independent column vectors on those collocation points. Furthermore, since $(F_1, F_2, F_3) = (0, 0, F_3)$, (3.24) shows that the system matrix in the quaternion harmonic approximation is invertible if and only if F_3 is invertible. This is due to the fact that in this case, the nonzero blocks in (3.24) are $\pm F_3$ on the anti-diagonal.*

REMARK 3.9. *For flat triangles in the xy -plane, $\nabla H^{(l,m)} \cdot \boldsymbol{\nu} = F^{(l,m)}(x, y)$ ($1 \leq m \leq l \leq p$) span the same subspace as the standard p th order monomial basis $\{x^i y^j | 0 \leq i + j \leq p - 1\}$. This is used in the single layer potential density approximation (3.31).*

For an arbitrary nonflat triangular patch in three dimensions it is rather difficult to construct a set of complete and linearly independent harmonic polynomial basis so that the resulting linear system (3.22) is always solvable. However, all surface patches become closer and closer to being flat when the patch size approaches zero. Thus, the harmonic basis functions that work for flat triangles seem to be a good choice even for a general curvilinear triangular patch. In practice, we observe that such basis functions lead to an invertible linear system in (3.22) with the desired convergence order p , even when the patch is relatively large and nonflat.

3.3. New treatment of the Laplace single layer potential. In this section, we present a more natural reduction of the Laplace single layer potential (SLP) to 1-forms, which requires a scalar harmonic density approximation and a single DLP density approximation. Since the cost of quaternion approximation and subsequent calculations is much more than that of the scalar part, the cost of evaluating the SLP by our scheme is close to that of the DLP. For comparison, the scheme in [79, 80] requires three quaternion density approximations for the SLP evaluation.

LEMMA 3.10. *Suppose that u and v are solutions to the Laplace equation. Suppose further that P is a contractible patch on a smooth oriented surface S in three dimensions. Then the 2-form*

$$(3.25) \quad (u \nabla v - v \nabla u) \cdot \boldsymbol{\nu} da(\mathbf{r})$$

is closed, and thus exact on P , where $da(\mathbf{r})$ is the area differential.

Proof. This simply follows from

$$(3.26) \quad \nabla \cdot (u \nabla v - v \nabla u) = u \Delta v - v \Delta u = 0. \quad \square$$

The following corollary is immediate.

COROLLARY 3.11. *Suppose that v is a harmonic function, i.e., $\Delta v = 0$. Then the 2-form*

$$(3.27) \quad \chi(\mathbf{r}', \mathbf{r}) = (G(\mathbf{r}', \mathbf{r}) \nabla H(\mathbf{r}) - H(\mathbf{r}) \nabla G(\mathbf{r}', \mathbf{r})) \cdot \boldsymbol{\nu}(\mathbf{r}) da(\mathbf{r})$$

is closed, i.e., $d\chi(\mathbf{r}', \mathbf{r}) = 0$ for $\mathbf{r} \neq \mathbf{r}'$.

Substituting $v = H^{(l,m)}$ with $H^{(l,m)}$ defined in (3.6) into (3.27), we obtain a closed and exact 2-form $\chi^{(l,m)}$ defined by the formula

$$(3.28) \quad \chi^{(l,m)}(\mathbf{r}', \mathbf{r}) = (G(\mathbf{r}', \mathbf{r}) \nabla H^{(l,m)}(\mathbf{r}) - H^{(l,m)}(\mathbf{r}) \nabla G(\mathbf{r}', \mathbf{r})) \cdot \boldsymbol{\nu}(\mathbf{r}) da(\mathbf{r}).$$

We denote the 1-forms whose exterior derivative are $\chi^{(l,m)}$ by $\psi^{(l,m)}$, that is,

$$(3.29) \quad \chi^{(l,m)}(\mathbf{r}', \mathbf{r}) = d\psi^{(l,m)}(\mathbf{r}', \mathbf{r}),$$

and by the Stokes theorem,

$$(3.30) \quad \int_P \chi^{(l,m)}(\mathbf{r}', \mathbf{r}) = \int_{\partial P} \psi^{(l,m)}(\mathbf{r}', \mathbf{r}).$$

THEOREM 3.12. *Suppose that P is a contractable patch in \mathbb{R}^3 and $\mathbf{r}^{(i,j)}$ are a set of n_p collocation points on P . Suppose further that the density in the Laplace single layer potential (1.1) is approximated by*

$$(3.31) \quad \sigma(\mathbf{r}) \approx \sum_{l=1}^p \sum_{m=1}^l \nabla H^{(l,m)}(\mathbf{r}) \cdot \boldsymbol{\nu}(\mathbf{r}) d^{(l,m)},$$

where $d^{(l,m)}$ are scalar coefficients determined by the following $n_p \times n_p$ linear system:

$$(3.32) \quad \sum_{l=1}^p \sum_{m=1}^l \nabla H^{(l,m)}(\mathbf{r}^{(i,j)}) \cdot \boldsymbol{\nu}(\mathbf{r}^{(i,j)}) d^{(l,m)} = \sigma(\mathbf{r}^{i,j}).$$

Let $\rho(\mathbf{r})$ be an intermediate DLP density defined by the formula

$$(3.33) \quad \rho(\mathbf{r}) = \sum_{l,m} H^{(l,m)}(\mathbf{r}) d^{(l,m)},$$

and approximate $\rho(\mathbf{r})$ using quaternion basis $(0, \nabla H^{(l,m)})$ (cf. (2.24)):

$$(3.34) \quad (\rho(\mathbf{r}), \mathbf{0}) \approx \sum_{l,m} (0, \nabla H^{(l,m)}(\mathbf{r})) g^{(l,m)}.$$

Then the Laplace single layer potential on P can be reduced to the evaluation of 1-forms as follows:

$$(3.35) \quad \begin{aligned} \mathcal{S}[\sigma](\mathbf{r}') &= \int_P G(\mathbf{r}', \mathbf{r}) \sigma(\mathbf{r}) da(\mathbf{r}) \\ &= \sum_{l,m} \int_{\partial P} \left(\psi^{(l,m)}(\mathbf{r}', \mathbf{r}) d^{(l,m)} - \left[\beta^{(l,m)}(\mathbf{r}', \mathbf{r}) g^{(l,m)} \right]_0 \right), \end{aligned}$$

where $\psi^{(l,m)}$ is defined in (3.29) and $\beta^{(l,m)}$ is defined in (2.22).

Proof. Combining (3.28) and (3.31), we obtain

$$(3.36) \quad \begin{aligned} G(\mathbf{r}', \mathbf{r})\sigma(\mathbf{r})d\mathbf{a}(\mathbf{r}) &\approx \sum_{l,m} G(\mathbf{r}', \mathbf{r})\nabla H^{(l,m)}(\mathbf{r}) \cdot \boldsymbol{\nu}(\mathbf{r})d^{(l,m)}d\mathbf{a}(\mathbf{r}) \\ &= \sum_{l,m} \chi^{(l,m)}(\mathbf{r}', \mathbf{r})d^{(l,m)} + \nabla G(\mathbf{r}', \mathbf{r}) \cdot \boldsymbol{\nu}(\mathbf{r})\rho(\mathbf{r})d\mathbf{a}(\mathbf{r}). \end{aligned}$$

Note that the second term on the right hand side of (3.36) is the Laplace double layer potential differential. Thus, using the quaternion approximation (3.34) and Lemma 2.3, we have

$$(3.37) \quad (0, \nabla G(\mathbf{r}', \mathbf{r}))(0, \boldsymbol{\nu}(\mathbf{r}))\rho(\mathbf{r})d\mathbf{a}(\mathbf{r}) \approx \sum_{l,m} \alpha^{(l,m)}(\mathbf{r}', \mathbf{r})g^{(l,m)},$$

with exact quaternion 2-forms $\alpha^{(l,m)}$ defined in (2.21).

Combining (3.36) – (3.37), we obtain

$$(3.38) \quad G(\mathbf{r}', \mathbf{r})\sigma(\mathbf{r})d\mathbf{a}(\mathbf{r}) \approx \sum_{l,m} \chi^{(l,m)}(\mathbf{r}', \mathbf{r})d^{(l,m)} - \sum_{l,m} \left[\alpha^{(l,m)}(\mathbf{r}', \mathbf{r})g^{(l,m)} \right]_0.$$

Finally, combining (2.22), (3.29), (3.30), and (3.38), we obtain (3.35). \square

In other words, the evaluation of the single layer potential is carried out by a scalar approximation to the original density in (3.31), a quaternion approximation (3.34) to the intermediate DLP density in (3.33), and then reduction to line integrals by the general Stokes theorem.

REMARK 3.13. Equation (3.35) is similar to the treatment of the Laplace single layer potential in two dimensions in [40, 41], where one evaluates the integrals involving the logarithmic kernel via the formula

$$(3.39) \quad \int_a^b \log(\tau - z_t)\tau^{n-1}d\tau = \frac{1}{n} \log(\tau - z_t)\tau^n \Big|_a^b - \frac{1}{n} \int_a^b \frac{\tau^n}{\tau - z_t} d\tau.$$

3.4. Singularity preserving 1-forms. The differential 1-forms $\beta^{(l,m)}$ in (2.28) and $\psi^{(l,m)}$ in (3.35) are not unique. Indeed, different choice of the reference point \mathbf{p} in (2.5) leads to different 1-forms. In [79, 80], $\mathbf{p} = \mathbf{0}$ and the singularity in the resulting 1-forms for the double layer potential is fairly complicated (see Appendix B of [80] for explicit expressions). These nearly singular line integrals often require expensive adaptive integration when the target point \mathbf{r}' is close to the boundary curves of P . We propose to use \mathbf{r}' as the reference point when constructing $\beta^{(l,m)}$ and $\psi^{(l,m)}$. The advantage of using $\mathbf{p} = \mathbf{r}'$ in (2.5) is that the resulting 1-forms have the same singularity as the Green's function and its derivatives, i.e., $1/|\mathbf{r}' - \mathbf{r}|^n$ for some positive integer n . The singularity-swap quadrature [1] can then be used to evaluate these line integrals via analytical recurrence after polynomial approximation of the density and a root-finding step. In other words, 1-forms are reduced to 0-forms and the need of adaptive integration is removed.

We now derive these target-centered 1-forms. The translation of harmonic polynomials becomes straightforward when complex solid harmonic polynomials are used. Thus, we introduce

$$(3.40) \quad S^{(l,m)}(\mathbf{r}) = S^{(l,m)}(x, y, z) = R_l^m(y, z, x).$$

Combining (3.1) and (3.6), we have

$$(3.41) \quad H^{(l,m)}(\mathbf{r}) = \sqrt{2} \operatorname{Im}(S^{(l,m)}(\mathbf{r})).$$

The translation of $S^{(l,m)}$ is the same as that of R_l^m in (2.13), which leads to

$$(3.42) \quad \begin{aligned} S^{(l,m)}(\mathbf{r}' + t(\mathbf{r} - \mathbf{r}')) &= \sum_{j=0}^l \sum_{k=-j}^j S^{(j,k)}(t\mathbf{r}) S^{(l-j,m-k)}((1-t)\mathbf{r}') T_{jk,lm} \\ &= \sum_{j=0}^l t^j (1-t)^{l-j} \sum_{k=-j}^j S^{(j,k)}(\mathbf{r}) S^{(l-j,m-k)}(\mathbf{r}') T_{jk,lm}. \end{aligned}$$

Instead of real differential 2-forms $\alpha^{(l,m)}$ in (2.21) for the DLP, we consider complex differential 2-forms

$$(3.43) \quad \tilde{\alpha}^{(l,m)}(\mathbf{r}', \mathbf{r}) = (0, \nabla G(\mathbf{r}', \mathbf{r}))(0, \boldsymbol{\nu}(\mathbf{r}))(0, \nabla S^{(l,m)}(\mathbf{r})) da(\mathbf{r}).$$

THEOREM 3.14 (DLP 1-forms). *Let $\tilde{\alpha}^{(l,m)}$ be the complex differential 2-forms defined in (3.43). Let P be a triangular patch on S . Suppose that the complex differential 1-forms $\tilde{\beta}^{(l,m)}$ are defined by*

$$(3.44) \quad \tilde{\beta}^{(l,m)}(\mathbf{r}', \mathbf{r}) = \frac{1}{4\pi} \sum_{j=2}^l C_{j,l} \sum_{k=-j}^j q^{(j,k)}(\mathbf{r}', \mathbf{r}) S^{(l-j,m-k)}(\mathbf{r}') T_{jk,lm},$$

where

$$(3.45) \quad C_{j,l} = \int_0^1 t^{j-2} (1-t)^{l-j} dt = \frac{(j-2)!(l-j)!}{(l-1)!},$$

and the quaternion 1-forms $q^{(j,k)}$ are given by the formula

$$(3.46) \quad q^{(j,k)}(\mathbf{r}', \mathbf{r}) = - \left(0, d \left(\frac{\mathbf{r}' - \mathbf{r}}{|\mathbf{r}' - \mathbf{r}|} \right) \right) \left(0, \nabla S^{(j,k)}(\mathbf{r}) \right).$$

Suppose further that

$$(3.47) \quad \gamma^{(l,m)}(\mathbf{r}', \mathbf{r}) = \frac{1}{4\pi} \omega(\mathbf{r}', \mathbf{r})(0, \nabla S^{(l,m)}(\mathbf{r}')),$$

where $\omega = (\omega_0, \boldsymbol{\omega})$ is a quaternion 1-form defined by

$$(3.48) \quad \omega_0(\mathbf{r}', \mathbf{r}) = \frac{((\mathbf{r}' - \mathbf{r}) \times \mathbf{u}) \cdot d\mathbf{r}}{|\mathbf{r}' - \mathbf{r}|(|\mathbf{r}' - \mathbf{r}| + \mathbf{u} \cdot (\mathbf{r}' - \mathbf{r}))},$$

$$(3.49) \quad \boldsymbol{\omega}(\mathbf{r}', \mathbf{r}) = - \frac{d\mathbf{r}}{|\mathbf{r}' - \mathbf{r}|},$$

with \mathbf{u} a fixed unit vector satisfying the property that $\mathbf{u} \cdot \boldsymbol{\nu}(\mathbf{r}) \leq 0$ for any $\mathbf{r} \in P$. Then

$$(3.50) \quad d \left(\tilde{\beta}^{(l,m)}(\mathbf{r}', \mathbf{r}) + \gamma^{(l,m)}(\mathbf{r}', \mathbf{r}) \right) = \tilde{\alpha}^{(l,m)}(\mathbf{r}', \mathbf{r}).$$

Proof. Straightforward calculation shows that

$$(3.51) \quad \begin{aligned} G(\mathbf{r}', \mathbf{r}' + t(\mathbf{r} - \mathbf{r}')) &= \frac{1}{4\pi t |\mathbf{r}' - \mathbf{r}|}, \\ \nabla G(\mathbf{r}', \mathbf{r}' + t(\mathbf{r} - \mathbf{r}')) &= \frac{\mathbf{r}' - \mathbf{r}}{4\pi t^2 |\mathbf{r}' - \mathbf{r}|^3}, \end{aligned}$$

and

$$(3.52) \quad \begin{aligned} \tilde{\alpha}^{(l,m)}(\mathbf{r}', \mathbf{r}) &= \left((\nabla G \times \nabla S^{(l,m)}) \cdot \boldsymbol{\nu}, -(\nabla G \cdot \boldsymbol{\nu}) \nabla S^{(l,m)} \right. \\ &\quad \left. + (\nabla G \times \boldsymbol{\nu}) \times \nabla S^{(l,m)} \right) da(\mathbf{r}), \end{aligned}$$

Note that $1/t^2$ appears in $\nabla G(\mathbf{r}', \mathbf{r}' + t(\mathbf{r} - \mathbf{r}'))$ because G is singular when $\mathbf{r} = \mathbf{r}'$. Thus, in order to apply (2.5) with $\mathbf{p} = \mathbf{r}'$, the density must be equal to zero at $t = 0$. For this, we split $\tilde{\alpha}^{(l,m)}$ into two terms:

$$(3.53) \quad \begin{aligned} \tilde{\alpha}^{(l,m)}(\mathbf{r}', \mathbf{r}) &= (0, \nabla G(\mathbf{r}', \mathbf{r}))(0, \boldsymbol{\nu}(\mathbf{r}))(0, \mathring{\nabla} S^{(l,m)}(\mathbf{r})) da(\mathbf{r}) \\ &\quad + (0, \nabla G(\mathbf{r}', \mathbf{r}))(0, \boldsymbol{\nu}(\mathbf{r}))(0, \nabla S^{(l,m)}(\mathbf{r}')) da(\mathbf{r}), \end{aligned}$$

where

$$(3.54) \quad \mathring{\nabla} S^{(l,m)}(\mathbf{r}) = \nabla S^{(l,m)}(\mathbf{r}) - \nabla S^{(l,m)}(\mathbf{r}'),$$

that is, we subtract the constant term so that $\mathring{\nabla} S^{(l,m)}(\mathbf{r}') = \mathbf{0}$. Now, (3.42) leads to (3.55)

$$\begin{aligned} \mathring{\nabla} S^{(l,m)}(\mathbf{r}' + t(\mathbf{r} - \mathbf{r}')) &= \sum_{j=2}^l t^{j-1} (1-t)^{l-j} \sum_{k=-j}^j \nabla S^{(j,k)}(\mathbf{r}) S^{(l-j, m-k)}(\mathbf{r}') T_{jk, lm} \\ &\quad + ((1-t)^{l-1} - 1) \sum_{k=-1}^1 \nabla S^{(1,k)} S^{(l-1, m-k)}(\mathbf{r}') T_{1k, lm}, \end{aligned}$$

where we have pulled out the $j = 1$ terms from the first summation on the right hand side of (3.55). We first calculate the contribution from the first summation on the right hand side of (3.55). Combining (2.5), (3.51), (3.43), and (3.55), we obtain the expression for $\tilde{\beta}^{(l,m)}$ given by (3.44)–(3.46). Applying integration by parts along ∂P , we obtain an alternative expression for $q^{(j,k)}$ in (3.46):

$$(3.56) \quad q^{(j,k)}(\mathbf{r}', \mathbf{r}) = \left(0, \frac{\mathbf{r}' - \mathbf{r}}{|\mathbf{r}' - \mathbf{r}|} \right) \left(0, d(\nabla S^{(j,k)}(\mathbf{r})) \right).$$

And it is easy to see that the contribution from the $j = 1$ terms on the right hand side of (3.55) is exactly zero due to the fact that $d(\nabla S^{1,k}(\mathbf{r})) = 0$. Thus, we have

$$(3.57) \quad d\tilde{\beta}^{(l,m)}(\mathbf{r}', \mathbf{r}) = (0, \nabla G(\mathbf{r}', \mathbf{r}))(0, \boldsymbol{\nu}(\mathbf{r}))(0, \mathring{\nabla} S^{(l,m)}(\mathbf{r})) da(\mathbf{r}).$$

DLP 1-forms for constant density. We now derive expressions for $\gamma^{(l,m)}$ in (3.50). It is clear that $\nabla S^{(l,m)}(\mathbf{r}')$ is a constant vector with respect to the integration variable \mathbf{r} . And it is easy to verify that

$$(3.58) \quad (0, \nabla G(\mathbf{r}', \mathbf{r}))(0, \boldsymbol{\nu}(\mathbf{r})) da(\mathbf{r}) = (-\nabla G(\mathbf{r}', \mathbf{r}) \cdot \boldsymbol{\nu}(\mathbf{r}), \nabla G(\mathbf{r}', \mathbf{r}) \times \boldsymbol{\nu}(\mathbf{r})) da(\mathbf{r})$$

is closed and exact. Thus, we have (3.47). Direct calculation shows that

$$(3.59) \quad \frac{1}{4\pi} d\omega = \nabla G(\mathbf{r}', \mathbf{r}) \times \boldsymbol{\nu}(\mathbf{r}) da(\mathbf{r}).$$

Now, it is well-known that $-\int_P \nabla \frac{1}{|\mathbf{r}' - \mathbf{r}|} \cdot \boldsymbol{\nu}(\mathbf{r}) da(\mathbf{r})$ is the solid angle of the patch P with respect to the target point \mathbf{r}' (see, for example, [2, 3, 52]). And (3.48) can be found in [2] with

$$(3.60) \quad \frac{1}{4\pi} d\omega_0 = -\nabla G(\mathbf{r}', \mathbf{r}) \cdot \boldsymbol{\nu}(\mathbf{r}) da(\mathbf{r}). \quad \square$$

REMARK 3.15. By (3.41), it follows that the real 1-forms $\beta^{(l,m)}$ in (2.22) are given by

$$(3.61) \quad \beta^{(l,m)}(\mathbf{r}', \mathbf{r}) = \sqrt{2} \operatorname{Im} \left(\tilde{\beta}^{(l,m)}(\mathbf{r}', \mathbf{r}) + \gamma^{(l,m)}(\mathbf{r}', \mathbf{r}) \right).$$

Similarly, we consider the following complex 2-forms for the SLP rather than the real 2-forms $\chi^{(l,m)}$ in (3.28):

$$(3.62) \quad \tilde{\chi}^{(l,m)}(\mathbf{r}', \mathbf{r}) = (G(\mathbf{r}', \mathbf{r}) \nabla S^{(l,m)}(\mathbf{r}) - \nabla G(\mathbf{r}', \mathbf{r}) S^{(l,m)}(\mathbf{r})) \cdot \boldsymbol{\nu} da(\mathbf{r}).$$

THEOREM 3.16 (SLP 1-forms). Let $\tilde{\chi}^{(l,m)}$ be complex differential 2-forms defined by (3.62). Suppose that the complex differential 1-forms $\tilde{\psi}^{(l,m)}$ are defined by

$$(3.63) \quad \tilde{\psi}^{(l,m)}(\mathbf{r}', \mathbf{r}) = \frac{1}{4\pi} \sum_{j=1}^l D_{j,l} \sum_{k=-j}^j v^{(j,k)}(\mathbf{r}', \mathbf{r}) S^{(l-j,m-k)}(\mathbf{r}') T_{jk,lm},$$

where

$$(3.64) \quad D_{j,l} = \int_0^1 t^{j-1} (1-t)^{l-j} dt = \frac{(j-1)!(l-j)!}{l!},$$

and

$$(3.65) \quad v^{(j,k)}(\mathbf{r}', \mathbf{r}) = \frac{1}{|\mathbf{r}' - \mathbf{r}|} \left[(\mathbf{r}' - \mathbf{r}) \times \nabla S^{(j,k)}(\mathbf{r}) \right] \cdot d\mathbf{r}.$$

Then

$$(3.66) \quad d \left(\tilde{\psi}^{(l,m)}(\mathbf{r}', \mathbf{r}) + S^{(l,m)}(\mathbf{r}') \omega_0(\mathbf{r}', \mathbf{r}) \right) = \tilde{\chi}^{(l,m)}(\mathbf{r}', \mathbf{r}),$$

where ω_0 is given by (3.48).

Proof. In order to apply (2.5), we split $\tilde{\chi}^{(l,m)}$ into two terms:

$$(3.67) \quad \begin{aligned} \tilde{\chi}^{(l,m)}(\mathbf{r}', \mathbf{r}) &= (G(\mathbf{r}', \mathbf{r}) \nabla S^{(l,m)}(\mathbf{r}) - \nabla G(\mathbf{r}', \mathbf{r}) \mathring{S}^{(l,m)}(\mathbf{r})) \cdot \boldsymbol{\nu} da(\mathbf{r}) \\ &\quad - S^{(l,m)}(\mathbf{r}') \nabla G(\mathbf{r}', \mathbf{r}) \cdot \boldsymbol{\nu} da(\mathbf{r}), \end{aligned}$$

where

$$(3.68) \quad \mathring{S}^{(l,m)}(\mathbf{r}) = S^{(l,m)}(\mathbf{r}) - S^{(l,m)}(\mathbf{r}').$$

Consider first 1-forms for the first term on the right hand side of (3.67). It follows from (3.42) that

$$(3.69) \quad \begin{aligned} \mathring{S}^{(l,m)}(\mathbf{r}' + t(\mathbf{r} - \mathbf{r}')) &= \sum_{j=1}^l t^j (1-t)^{l-j} \sum_{k=-j}^j S^{(j,k)}(\mathbf{r}) S^{(l-j,m-k)}(\mathbf{r}') T_{jk,lm} \\ &\quad + ((1-t)^l - 1) S^{(0,0)} S^{(l,m)}(\mathbf{r}') T_{00,lm}, \\ \nabla S^{(l,m)}(\mathbf{r}' + t(\mathbf{r} - \mathbf{r}')) &= \sum_{j=1}^l t^{j-1} (1-t)^{l-j} \sum_{k=-j}^j \nabla S^{(j,k)}(\mathbf{r}) S^{(l-j,m-k)}(\mathbf{r}') T_{jk,lm}. \end{aligned}$$

Combining (2.5), (3.51), (3.67), and (3.69), we obtain the expression for $\tilde{\psi}^{(l,m)}$ given by (3.63)–(3.65). For the second term on the right hand side of (3.67), it is easy to see that

$$(3.70) \quad -S^{(l,m)}(\mathbf{r}') \nabla G(\mathbf{r}', \mathbf{r}) \cdot \boldsymbol{\nu} da(\mathbf{r}) = S^{(l,m)}(\mathbf{r}') d\omega_0,$$

with ω_0 defined in (3.48). \square

REMARK 3.17. By (3.41), it follows that the real 1-forms $\psi^{(l,m)}$ in (3.29) are given by

$$(3.71) \quad \psi^{(l,m)}(\mathbf{r}', \mathbf{r}) = \sqrt{2} \operatorname{Im} \left(\tilde{\psi}^{(l,m)}(\mathbf{r}', \mathbf{r}) + S^{(l,m)}(\mathbf{r}') \omega_0(\mathbf{r}', \mathbf{r}) \right).$$

3.5. 1-to-0 form conversion. We now present some details on the evaluation of line integrals (i.e., integral of 1-forms) via the singularity-swap quadrature in [1]. Pulling out the target-dependent part from the 1-forms in (3.44)–(3.49) for the DLP and (3.63)–(3.65) for the SLP, we observe that the following line integrals need to be calculated:

$$(3.72) \quad \begin{aligned} Q^{(j,k)}(\mathbf{r}') &= \int_{\partial P} q^{(j,k)}(\mathbf{r}', \mathbf{r}) = - \int_{\partial P} \left(0, d \left(\frac{\mathbf{r}' - \mathbf{r}}{|\mathbf{r}' - \mathbf{r}|} \right) \right) \left(0, \nabla S^{(j,k)}(\mathbf{r}) \right), \\ \Omega(\mathbf{r}') &= \int_{\partial P} \boldsymbol{\omega}(\mathbf{r}', \mathbf{r}) = - \int_{\partial P} \frac{d\mathbf{r}}{|\mathbf{r}' - \mathbf{r}|}, \\ V^{(j,k)}(\mathbf{r}') &= \int_{\partial P} v^{(j,k)}(\mathbf{r}', \mathbf{r}) = \int_{\partial P} \frac{1}{|\mathbf{r}' - \mathbf{r}|} \left[(\mathbf{r}' - \mathbf{r}) \times \nabla S^{(j,k)}(\mathbf{r}) \right] \cdot d\mathbf{r}, \end{aligned}$$

and

$$(3.73) \quad \Omega_0 = \int_{\partial P} \omega_0(\mathbf{r}', \mathbf{r}) = \int_{\partial P} \frac{((\mathbf{r}' - \mathbf{r}) \times \mathbf{u}) \cdot d\mathbf{r}}{|\mathbf{r}' - \mathbf{r}| (|\mathbf{r}' - \mathbf{r}| + \mathbf{u} \cdot (\mathbf{r}' - \mathbf{r}))}.$$

We will use $V^{(j,k)}$ to illustrate the steps in the evaluation of line integrals in (3.72). For a smooth triangular patch P , its boundary ∂P consists of three smooth curves. Denote one such boundary curve by Γ , and assume that the parameterization of Γ induced by the parameterization of P is $\mathbf{r}(t)$ with $t \in [-1, 1]$. Then we only need to consider the evaluation of the following integral:

$$(3.74) \quad I^{(j,k)}(\mathbf{r}') = \int_{-1}^1 \frac{1}{|\mathbf{r}' - \mathbf{r}(t)|} \left[(\mathbf{r}' - \mathbf{r}(t)) \times \nabla S^{(j,k)}(\mathbf{r}(t)) \right] \cdot \frac{d\mathbf{r}(t)}{dt} dt.$$

As discussed in subsection 2.4, the above integral can be written as

$$(3.75) \quad I^{(j,k)}(\mathbf{r}') = \int_{-1}^1 \frac{F(t)}{((t-t_0)(t-\bar{t}_0))^{1/2}} dt,$$

where t_0 is a complex root satisfying (2.18) and

$$(3.76) \quad F(t) = \left[(\mathbf{r}' - \mathbf{r}(t)) \times \nabla S^{(j,k)}(\mathbf{r}(t)) \right] \cdot \frac{d\mathbf{r}(t)}{dt} \frac{|t - t_0|}{|\mathbf{r}(t) - \mathbf{r}'|}.$$

For a fixed target point \mathbf{r}' , we approximate $F(t)$ by its polynomial interpolant with, say, the \tilde{p} Gauss-Legendre nodes t_i ($i = 1, \dots, \tilde{p}$) as the interpolation nodes. That is,

$$(3.77) \quad F(t) = \sum_{i=0}^{\tilde{p}-1} \tilde{c}_i t^i, \quad \tilde{c} = UF,$$

where

$$(3.78) \quad \tilde{c} = \begin{bmatrix} \tilde{c}_0 \\ \vdots \\ \tilde{c}_{\tilde{p}-1} \end{bmatrix}, \quad F = \begin{bmatrix} F(t_1) \\ \vdots \\ F(t_{\tilde{p}}) \end{bmatrix}, \quad U = \begin{bmatrix} 1 & t_1 & \cdots & t_1^{\tilde{p}-1} \\ \vdots & \vdots & \vdots & \vdots \\ 1 & t_{\tilde{p}} & \cdots & t_{\tilde{p}}^{\tilde{p}-1} \end{bmatrix}^{-1}.$$

Here, \tilde{p} should be slightly greater than p in order to take the geometric variation and the smooth factor $|t - t_0|/|\mathbf{r}(t) - \mathbf{r}'|$ into account. In practice, we observe that $\tilde{p} = p + 5$ or $\tilde{p} = 2p$ works well. The integrals

$$(3.79) \quad \mathcal{I}_i(\mathbf{r}') = \int_{-1}^1 \frac{t^i}{((t - t_0)(t - \bar{t}_0))^{1/2}} dt$$

can be calculated by a recurrence relation (see [1] for details). Thus,

$$(3.80) \quad I^{(j,k)}(\mathbf{r}') = \sum_{i=0}^{\tilde{p}-1} \tilde{c}_i \mathcal{I}_i = \mathcal{I}(\mathbf{r}')^T U F(\mathbf{r}'), \quad \mathcal{I}(\mathbf{r}')^T = [\mathcal{I}_0(\mathbf{r}') \quad \dots \quad \mathcal{I}_{\tilde{p}-1}(\mathbf{r}')].$$

Note that the matrix U can be precomputed and stored since it is independent of \mathbf{r}' .

After quantities such as $I^{(j,k)}$ have been calculated, the line integrals associated with the DLP and SLP can be calculated easily. For example, the integrals of $\tilde{\beta}^{(l,m)}$ in (3.44) are computed by

(3.81)

$$I[\tilde{\beta}^{(l,m)}](\mathbf{r}') = \int_{\partial P} \tilde{\beta}^{(l,m)}(\mathbf{r}', \mathbf{r}) = \frac{1}{4\pi} \sum_{j=2}^l C_{j,l} \sum_{k=-j}^j Q^{(j,k)}(\mathbf{r}') S^{(l-j,m-k)}(\mathbf{r}') T_{jk,lm}.$$

REMARK 3.18. *Straightforward calculation shows that (3.46) contains both $1/|\mathbf{r}' - \mathbf{r}|$ and $1/|\mathbf{r}' - \mathbf{r}|^3$ near-singularities. If we use (3.56) to calculate $Q^{(j,k)}$, then we only need to deal with the $1/|\mathbf{r}' - \mathbf{r}|$ near-singularity.*

REMARK 3.19. *The solid angle Ω_0 in (3.73) does not have a clean $1/|\mathbf{r}' - \mathbf{r}|^m$ near-singularity. However, if we pull out the factor $|\mathbf{r}' - \mathbf{r}|^2$ from the denominator in (3.73), we obtain $(1 + \cos \varphi)$ with φ the angle between \mathbf{u} and $\mathbf{r}' - \mathbf{r}$. By the condition stated in Theorem 3.14 on \mathbf{u} , $\cos \varphi$ is greater than 0 in most cases. Thus, the extra factor $(1 + \cos \varphi)$ can be treated by a slight upsampling or very mild adaptive integration.*

3.6. Evaluation of the normal derivative of the single layer potential.

We denote the quaternions $(0, \boldsymbol{\nu}')$ and $(0, \boldsymbol{\nu})$ by ν' and ν , respectively. Since $\boldsymbol{\nu}$ is a unit vector, we have $\nu\bar{\nu} = 1$. In order to evaluate $\mathcal{S}'[\sigma](\mathbf{r}') = -\int_P \boldsymbol{\nu}' \cdot \nabla G(\mathbf{r}', \mathbf{r}) \sigma(\mathbf{r}) d\mathbf{a}(\mathbf{r})$, where ∇ is with respect to \mathbf{r} , we rewrite the integrand using quaternion algebra as follows:

$$(3.82) \quad \begin{aligned} \boldsymbol{\nu}' \cdot \nabla G(\mathbf{r}', \mathbf{r}) \sigma(\mathbf{r}) d\mathbf{a}(\mathbf{r}) &= [(0, \boldsymbol{\nu}')(0, \nabla G(\mathbf{r}', \mathbf{r})) \sigma(\mathbf{r}) d\mathbf{a}(\mathbf{r})]_0 \\ &= [\nu'(0, \nabla G(\mathbf{r}', \mathbf{r})) \nu (\bar{\nu} \sigma(\mathbf{r})) d\mathbf{a}(\mathbf{r})]_0. \end{aligned}$$

We observe that ν' depends on the target point \mathbf{r}' and thus can be pulled out the integration. We now treat $\bar{\nu} \sigma = (0, -\boldsymbol{\nu}(\mathbf{r})) \sigma(\mathbf{r})$ as a quaternion density, and approximate it via harmonic polynomials:

$$(3.83) \quad (0, \sigma(\mathbf{r}) \nu(\mathbf{r})) \approx \sum_{l=1}^p \sum_{m=1}^l (0, \nabla H^{(l,m)}(\mathbf{r})) w^{(l,m)}, \quad \mathbf{r} \in P.$$

And the linear system for obtaining the quaternion coefficient $c^{(l,m)}$ is given by

$$(3.84) \quad \sum_{l=1}^p \sum_{m=1}^l (0, \nabla H^{(l,m)}(\mathbf{r}^{(i,j)})) w^{(l,m)} = (0, \sigma(\mathbf{r}^{(i,j)}) \nu(\mathbf{r}^{(i,j)})), \quad 0 \leq i+j \leq p-1.$$

We observe that (3.83) is very similar to the quaternion harmonic density approximation (2.24) for the double layer potential, and that (3.84) has the same system matrix as (3.22) for the DLP evaluation. Thus, the evaluation of \mathcal{S}' is very close that of \mathcal{D} . The difference is that the right hand side in the density approximation is $(\mu, \mathbf{0})$ in (2.24) for \mathcal{D} , and $(0, \sigma \nu)$ in (3.83) for \mathcal{S}' . We also need to multiply the quaternion $\nu' = (0, \boldsymbol{\nu}')$ from left for \mathcal{S}' in postprocessing. In short, we have

$$(3.85) \quad \begin{aligned} \mathcal{S}'[\sigma](\mathbf{r}') &\approx \left[(0, \boldsymbol{\nu}') \sum_{l,m} \int_P \alpha^{(l,m)}(\mathbf{r}', \mathbf{r}) w^{(l,m)} \right]_0 \\ &= \left[(0, \boldsymbol{\nu}') \sum_{l,m} \int_{\partial P} \beta^{(l,m)}(\mathbf{r}', \mathbf{r}) w^{(l,m)} \right]_0, \end{aligned}$$

where $[\cdot]_0$ denotes the scalar part of the quaternion, 2-forms $\alpha^{(l,m)}$ are defined by (2.21), and 1-forms $\beta^{(l,m)}$ are defined by (2.22), whose calculation is discussed in detail in Theorem 3.14 and subsection 3.5.

3.7. Evaluation of the normal derivative of the double layer potential.

The normal derivative, or the gradient, of the double layer potential can be computed by differentiating the associated 1-forms. By combining (2.28), (3.44)–(3.49) and (3.61), we have

$$(3.86) \quad \begin{aligned} \mathcal{D}[\mu](\mathbf{r}') &\approx -\sum_{l,m} \int_{\partial P} [\beta^{(l,m)}(\mathbf{r}', \mathbf{r}) c^{(l,m)}]_0 \\ &= -\sqrt{2} \left[\sum_{l,m} \operatorname{Im} \left(\int_{\partial P} (\tilde{\beta}^{(l,m)}(\mathbf{r}', \mathbf{r}) + \gamma^{(l,m)}(\mathbf{r}', \mathbf{r})) \right) c^{(l,m)} \right]_0 \\ &:= -\sqrt{2} \left[\sum_{l,m} \operatorname{Im} \left(I[\tilde{\beta}^{(l,m)}](\mathbf{r}') + I[\gamma^{(l,m)}](\mathbf{r}') \right) c^{(l,m)} \right]_0. \end{aligned}$$

Here, $I[\tilde{\beta}^{(l,m)}]$ is given by (3.81) and $I[\gamma^{(l,m)}]$ is defined by the formula

$$(3.87) \quad I[\gamma^{(l,m)}](\mathbf{r}') = \int_{\partial P} \gamma^{(l,m)}(\mathbf{r}', \mathbf{r}) = \frac{1}{4\pi} \Omega(\mathbf{r}') (0, \nabla S^{(l,m)}(\mathbf{r}')),$$

where $\Omega(\mathbf{r}') = (\Omega_0(\mathbf{r}'), \mathbf{\Omega}(\mathbf{r}'))$ with Ω_0 and $\mathbf{\Omega}$ given by (3.73) and the second equation in (3.72), respectively. Product rule can then be applied to differentiate $\Omega(\mathbf{r}')$ and $\nabla S^{(l,m)}(\mathbf{r}')$ to obtain the derivatives of $I[\tilde{\beta}^{(l,m)}](\mathbf{r}')$ and $I[\gamma^{(l,m)}](\mathbf{r}')$. Straightforward calculation leads to the following expressions:

$$(3.88) \quad \begin{aligned} \frac{\partial Q^{(j,k)}(\mathbf{r}')}{\partial \boldsymbol{\nu}'} &= \int_{\partial P} \left(0, \frac{\boldsymbol{\nu}'}{|\mathbf{r}' - \mathbf{r}|} - \frac{(\boldsymbol{\nu}' \cdot (\mathbf{r}' - \mathbf{r}))(\mathbf{r}' - \mathbf{r})}{|\mathbf{r}' - \mathbf{r}|^3} \right) (0, d\nabla S^{(j,k)}(\mathbf{r})), \\ \frac{\partial \mathbf{\Omega}(\mathbf{r}')}{\partial \boldsymbol{\nu}'} &= \int_{\partial P} \frac{\boldsymbol{\nu}' \cdot (\mathbf{r}' - \mathbf{r}) d\mathbf{r}}{|\mathbf{r}' - \mathbf{r}|^3}, \\ \frac{\partial \Omega_0(\mathbf{r}')}{\partial \boldsymbol{\nu}'} &= \int_{\partial P} \frac{(\boldsymbol{\nu}' \times \mathbf{u}) \cdot d\mathbf{r}}{|\mathbf{r}' - \mathbf{r}|(|\mathbf{r}' - \mathbf{r}| + \mathbf{u} \cdot (\mathbf{r}' - \mathbf{r}))} - \frac{(\boldsymbol{\nu}' \cdot \mathbf{u})((\mathbf{r}' - \mathbf{r}) \times \mathbf{u}) \cdot d\mathbf{r}}{|\mathbf{r}' - \mathbf{r}|(|\mathbf{r}' - \mathbf{r}| + \mathbf{u} \cdot (\mathbf{r}' - \mathbf{r}))^2} \\ &\quad - \frac{(\boldsymbol{\nu}' \cdot (\mathbf{r}' - \mathbf{r}))((\mathbf{r}' - \mathbf{r}) \times \mathbf{u}) \cdot d\mathbf{r}}{|\mathbf{r}' - \mathbf{r}|^2(|\mathbf{r}' - \mathbf{r}| + \mathbf{u} \cdot (\mathbf{r}' - \mathbf{r}))^2} - \frac{(\boldsymbol{\nu}' \cdot (\mathbf{r}' - \mathbf{r}))((\mathbf{r}' - \mathbf{r}) \times \mathbf{u}) \cdot d\mathbf{r}}{|\mathbf{r}' - \mathbf{r}|^3(|\mathbf{r}' - \mathbf{r}| + \mathbf{u} \cdot (\mathbf{r}' - \mathbf{r}))}. \end{aligned}$$

We observe that both $\partial Q^{(j,k)}(\mathbf{r}')/\partial \boldsymbol{\nu}'$ and $\partial \mathbf{\Omega}(\mathbf{r}')/\partial \boldsymbol{\nu}'$ can be computed directly via the singularity-swap quadrature, while $\partial \Omega_0(\mathbf{r}')/\partial \boldsymbol{\nu}'$ can be computed via the singularity-swap quadrature with slight upsampling or mild adaptive integration.

4. Numerical algorithm. The following algorithm summarizes the steps in the evaluation of the Laplace double layer potential.

Close evaluation of the Laplace double layer potential

Input/output: Suppose that P is a smooth triangular patch on S (we assume that translation and rotation have been carried out so that three vertices of P are on the xy plane and the center of P is the origin), μ is the given DLP density, and \mathbf{r}' is the given target point. Let p be the polynomial approximation order on P and $n_p = p(p+1)/2$, and $\mathbf{r}^{(i,j)}$ ($1 \leq i+j \leq p$) be a set of interpolation/collocation nodes on P . Let \tilde{p} (say, $\tilde{p} = 2p$) be the polynomial approximation order on ∂P , and \mathbf{r}_i ($i = 1, \dots, 3\tilde{p}$) be a set of interpolation nodes on three edges of ∂P . Compute the DLP $\mathcal{D}[\mu](\mathbf{r}') = \int_P \nabla G(\mathbf{r}', \mathbf{r}) \cdot \boldsymbol{\nu}(\mathbf{r}) \mu(\mathbf{r}) da(\mathbf{r})$.

Step 1: For each source point $\mathbf{r}^{(i,j)}$ on P , compute $S^{(l,m)}(\mathbf{r}^{(i,j)})$ and $\nabla S^{(l,m)}(\mathbf{r}^{(i,j)})$ for all $1 \leq m \leq l \leq p$ via the recurrence relation (2.10). Construct the system matrix in (3.22). [This step depends only on sources. The cost of constructing the system matrix is $O(n_p^2) = O(p^4)$.]

Step 2: Solve the linear system (3.22) to obtain the quaternion coefficient vector $c^{(l,m)}$ for all $1 \leq m \leq l \leq p$. [This step depends only on sources. The cost of solving the $4n_p \times 4n_p$ linear system is $O((4n_p)^3) = O(p^6)$.]

Step 3: For each source point \mathbf{r}_i on ∂P , compute $S^{(l,m)}(\mathbf{r}_i)$ and $\nabla S^{(l,m)}(\mathbf{r}_i)$ for all $1 \leq m \leq l \leq p$ via the recurrence relation (2.10). [This step depends only on sources. The cost is $O(p^3)$.]

Step 4: For the target point \mathbf{r}' , compute $S^{(l,m)}(\mathbf{r}')$ and $\nabla S^{(l,m)}(\mathbf{r}')$ via the recurrence relation (2.10). [This step depends only on the target. The cost is $O(p^2)$.]

Step 5: For each edge on ∂P , find the value of t_0 for the given target \mathbf{r}' and compute \mathcal{I}_i in (3.79) for $0 \leq i \leq \tilde{p} - 1$ via the recurrence relation in [1]. [This step depends on the target and sources on ∂P . The cost is $O(p)$.]

Step 6: For the target point \mathbf{r}' , compute the line integrals $Q^{(j,k)}(\mathbf{r}')$ in (3.72) for all $1 \leq k \leq j \leq p$ using formulas similar to (3.80). [This step depends on the target and sources on ∂P . For each (j, k) pair, the work involves elementwise multiplication and a matrix-vector product. Thus, the cost of this step is $O(p^3)$.]

Step 7: For the target point \mathbf{r}' , compute the integrals $I[\tilde{\beta}^{(l,m)}](\mathbf{r}')$ in (3.81) for all $1 \leq m \leq l \leq p$. Also compute $I[\gamma^{(l,m)}](\mathbf{r}')$, the integrals of $\gamma^{(l,m)}$, for $\gamma^{(l,m)}$ defined in (3.47). [This step depends on the target and sources on ∂P . Using the fast translation scheme in Remark 2.2, the cost of this step is $O(p^3)$.]

Step 8: Compute the DLP by combining (2.28), (3.61), and (3.81). That is, compute

$$(4.1) \quad D^{(l,m)}(\mathbf{r}') = -\sqrt{2}\text{Im} \left(I[\tilde{\beta}^{(l,m)}](\mathbf{r}') + I[\gamma^{(l,m)}](\mathbf{r}') \right), \quad 1 \leq m \leq l \leq p,$$

then set

$$\mathcal{D}[\mu](\mathbf{r}') = \sum_{l,m} \left[D^{(l,m)}(\mathbf{r}') c^{(l,m)} \right]_0,$$

where $[\cdot]_0$ denotes the scalar part of the quaternion. [This is basically the evaluation of the quaternion product for two quaternion vectors. The cost of this step is $O(p^2)$.]

REMARK 4.1. The above algorithm works for self-interaction, near-interaction, and close evaluation outlined in section 1, providing a unified high-order scheme for all three interactions.

REMARK 4.2. The above algorithm assumes that the density is given. In the case of constructing the system matrix during the solve phase of integral equation methods, we first skip Step 2. Then instead of computing the quaternion dot product of $w^T c$ in Step 8, we compute $[w^T(\mathbf{r}')A^{-1}]_0$ to obtain a row vector corresponding to the given target \mathbf{r}' . Here, $w^T = [w^{(l,m)}], 1 \leq m \leq l \leq p$ is the quaternion row vector in (4.1), and A is the system matrix constructed in Step 1.

REMARK 4.3. (a) The evaluation of the single layer potential is similar, with additional scalar density approximation in (3.32) and calculation of integrals of 1-forms in (3.63). (b) The evaluation of the normal derivative of the SLP is almost identical. In Step 2, we solve the linear system (3.84) instead. In Step 8, we evaluate the last expression in (3.85). (c) The evaluation of the normal derivative of the DLP is almost identical. In Step 6, we also need to compute line integrals in (3.88) as well.

REMARK 4.4. In order to evaluate layer potentials for a collection of target points, we will need to divide the surface S into a collection of triangular patches and identify the targets that require special quadrature construction for each patch. These two steps are fairly standard in scientific computing and we omit the details. For example, the second step can be carried out using either an adaptive octree [66] or a k-d tree (see, for example, [63, 77]).

REMARK 4.5. The cost associated with each source patch is $O(p^6)$ with $O(p^2)$ source points on each patch. The cost associated with each target is $O(p^3)$. Thus, the total cost is $O(N_S p^4 + N_T p^3)$, with N_S the total number of source points on S and N_T the total number of target points requiring special quadrature. During the

solve phase of integral equation methods, N_T is a small factor of N_S (about 2 – 4 for reasonable geometries). The actual performance depends on many other factors such as the quality of implementation, memory latency, and prefactors in lower order terms.

5. Numerical examples. In this section, we illustrate the performance of our new quadrature scheme. The code is written in Fortran and compiled using gfortran 13.2.0 with optimization flag -O3. All experiments were run in single-threaded mode on a 3.60GHz AMD EPYC 9474F CPU.

For typical applications in integral equation methods, the evaluation of layer potentials is needed in two stages – the solve phase and the evaluation phase. Below, we will use the double layer potential as the example to explain the main steps, since other layer potentials can be treated in an almost identical manner. Denote the discrete matrix for the double layer potential by \mathbf{D} . During the solve phase, the double layer potential operator is a map from the boundary to itself and \mathbf{D} is a square matrix of size $N_S \times N_S$, where N_S is the total number of source points on the boundary. In order to apply \mathbf{D} fast to a given vector, it is necessary to split it into two parts:

$$(5.1) \quad \mathbf{D} = \mathbf{D}_{\text{smooth}} + \mathbf{D}_{\text{RRQ}},$$

where $\mathbf{D}_{\text{smooth}}$ is obtained by discretizing \mathcal{D} via smooth quadrature on each patch, and \mathbf{D}_{RRQ} is the quadrature correction part due to the singularity or near-singularity of the kernel. To be more precise, the weights in $\mathbf{D}_{\text{smooth}}$ depend only on the source points (i.e., functions of row indices only), while the weights in \mathbf{D}_{RRQ} depend on both sources and targets (i.e., functions of row and column indices). Since the quadrature weights depend only on sources, they can be combined with other source-dependent factors such as the jacobian into the given vector. This makes fast algorithms such as the FMM directly applicable to accelerate the matrix-vector product for $\mathbf{D}_{\text{smooth}}$ in $O(N_S)$ cost, with the prefactor depending on the prescribed precision. On the other hand, \mathbf{D}_{RRQ} is only nonzero for the targets that require our special quadrature for a given source patch. For typical geometries, the number of targets close to any patch is $O(1)$. Thus, \mathbf{D}_{RRQ} is a sparse matrix and the cost of the associated matrix-vector product is again $O(N_S)$, where the prefactor depends on the quadrature order p , the quality of triangulation, and the geometry of the boundary.

During the evaluation phase, layer potentials are evaluated on a set of volumetric grids. Thus, the discrete matrix \mathbf{D} is a rectangular matrix of size $N_T \times N_S$, where N_T is the total number of target points in the volume. For typical applications, the mesh size h for the discretization of the boundary surface and the volume is roughly equal to each other. Thus, $N_T = O(1/h^3)$ and $N_S = O(1/h^2)$. The application of \mathbf{D} to a known density is almost identical to the solve phase, as outlined above, with the cost of both parts being $O(N_S + N_T)$. The difference is that there are now many more target points, leading to different ratios in the computation time for these two parts. For both cases, we denote the apply time of $\mathbf{D}_{\text{smooth}}$ using the FMM by T_{FMM} and the time for building \mathbf{D}_{RRQ} by T_{RRQ} (the apply time of \mathbf{D}_{RRQ} is negligible). Similar to [32], We use the state-of-the-art software package FMM3D [25] for the fast multipole method. It is clear that T_{FMM} serves as an effective benchmark for evaluating the efficiency of our quadrature scheme. We remark here that the total time of the solve phase for iterative solvers such as GMRES [62] is approximately $T_{\text{RRQ}} + N_{\text{iter}}T_{\text{FMM}}$, where N_{iter} is the total number of GMRES iterations required to reach a prescribed tolerance.

The accuracy study is conducted in a similar manner. During the solve phase, the target points coincide with the source points on the boundary, involving only self-interactions and near interactions. In contrast, for the evaluation phase, the target points are generally located off the boundary within the volume—this is referred to as close evaluation. As discussed in [section 1](#), close evaluation is particularly challenging due to the limited availability of analytic techniques and because the target points can be arbitrarily close to the surface, requiring multiple levels of refinement in adaptive integration to resolve the near-singularity.

In the following examples, we consider the exterior Dirichlet problem for the Laplace equation:

$$(5.2) \quad \begin{aligned} \Delta u(\mathbf{r}') &= 0, & \mathbf{r}' \in D, \\ u(\mathbf{r}') &= f(\mathbf{r}'), & \mathbf{r}' \in S, \end{aligned}$$

where S is a smooth closed surface, and D is the exterior domain. In order to check the accuracy and convergence order, the boundary data f is chosen to be the restriction of an analytic solution on S , and the analytic solution is constructed as the superposition of the fundamental solutions with point sources lying on the interior of S :

$$(5.3) \quad u_{\text{exact}}(\mathbf{r}') = \sum_{j=1}^4 \frac{c_j}{|\mathbf{r}' - \mathbf{r}_j|}, \quad \mathbf{r}_j \in \bar{D}^c,$$

where \mathbf{r}_j ($j = 1, \dots, 4$) are their locations, and c_j are their strengths. Both \mathbf{r}_j and c_j are chosen randomly.

We use the so-called combined field integral representation [[15](#), Chapter 3]

$$(5.4) \quad u(\mathbf{r}') = (\mathcal{S} + \mathcal{D})[\sigma](\mathbf{r}'), \quad \mathbf{r}' \in D,$$

and the resulting boundary integral equation (BIE) is

$$(5.5) \quad \frac{1}{2}\sigma(\mathbf{r}') + (\mathcal{S} + \mathcal{D})[\sigma](\mathbf{r}') = f(\mathbf{r}'), \quad \mathbf{r}' \in S.$$

The boundary is divided into triangle patches, where the triangulation is carried out more or less uniformly in the parameter space. The Vioreanu-Rokhlin [[67](#)] nodes as the collocation points on each patch. The associated Vioreanu-Rokhlin quadrature is used to discretize the smooth interaction, and our quadrature scheme is used to discretize self- and near- interactions. The resulting linear system is solved via GMRES with prescribed tolerance 10^{-14} . A Cartesian tensor grid of equispaced points of certain size is placed on a rectangular box enclosing S and evaluations of the numerical solution to [\(5.2\)](#) are carried out at the grid points that are in the exterior domain. The relative l_∞ error is computed via the formula

$$(5.6) \quad E_\infty = \frac{\|u_{\text{num}} - u_{\text{exact}}\|_\infty}{\|u_{\text{exact}}\|_\infty}.$$

Note that E_∞ is the cumulative error from both the solve phase and the evaluation phase.

5.1. Study of accuracy and convergence order.

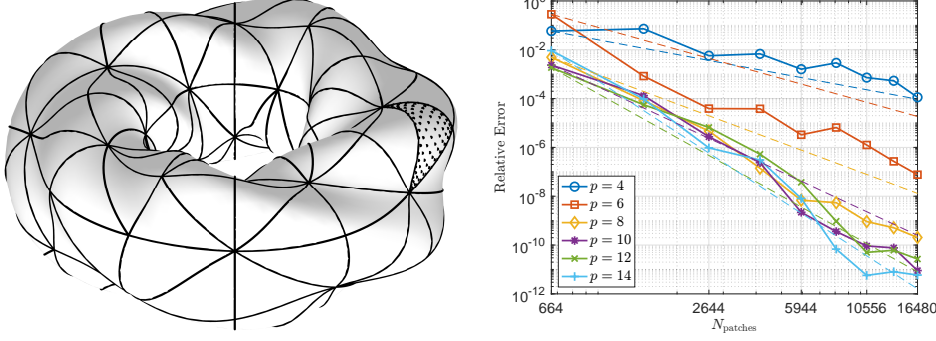


FIG. 5.1. Left: triangulated warped torus boundary. Right: relative l_∞ errors as functions of N_{patches} for various orders p .

5.1.1. A warped torus. The boundary S is a warped torus

$$(5.7) \quad \mathbf{r}(\theta, \phi) = \begin{bmatrix} (a + f(\theta, \phi) \cos(\theta)) \cos(\phi) \\ (a + f(\theta, \phi) \cos(\theta)) \sin(\phi) \\ f(\theta, \phi) \sin(\theta) \end{bmatrix}, \quad (\theta, \phi) \in [0, 2\pi]^2,$$

where $f(\theta, \phi) = b + \omega_c \cos(\omega_n \phi + \omega_m \theta)$. We set the parameters to $a = 1$, $b = 1/2$, $\omega_c = 0.065$, $\omega_n = 5$ and $\omega_m = 3$. See the image on the left side of Figure 5.1.

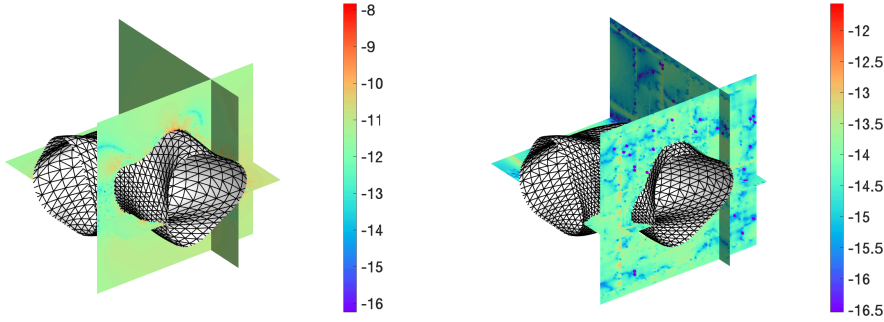


FIG. 5.2. Slice plots of \log_{10} of the pointwise relative errors for the warped torus. Left: $p = 8$, $n_\theta = 36$, $n_\phi = 72$. Right: $p = 14$, $n_\theta = 48$, $n_\phi = 96$.

The torus is discretized into $n_\theta \times n_\phi$ equi-sized rectangles, with each further subdivided into two equal triangular patches in the parameter space. Thus, the total number of patches N_{patches} is $2n_\theta n_\phi$. The equispaced tensor grid points are placed on the rectangular box $[-0.5, 2] \times [-0.5, 2] \times [-1.25, 1.25]$ and numerical solution is evaluated at 892932 points in the exterior of the warped torus. Table 5.1 shows E_∞ defined in (5.6) at sample values of $n_\theta \times n_\phi$ for $p = 4, 6, \dots, 14$. The image on the right side of Figure 5.1 plots these data points as a function of N_{patches} for these six values of p , with dashed lines showing the expected convergence order. Figure 5.2 plots pointwise relative errors at three orthogonal slices where such errors are maximal.

TABLE 5.1

Relative l_∞ errors E_∞ for the warped torus example at sample values of n_θ , n_ϕ , and p . The total number of patches is $N_{\text{patches}} = 2n_\theta n_\phi$ and the total number of discretization points is $N = N_{\text{patches}}p(p+1)/2$.

$n_\theta \times n_\phi \backslash p$	6	8	10	12	14
12×24	2.83e-01	4.96e-03	2.36e-03	1.86e-03	9.31e-03
18×36	8.37e-04	8.22e-05	1.32e-04	5.59e-05	9.62e-05
24×48	3.89e-05	4.69e-06	2.72e-06	6.57e-06	9.55e-07
30×60	3.82e-05	1.40e-07	2.37e-07	5.25e-07	3.04e-07
36×72	3.29e-06	6.87e-09	2.20e-09	3.68e-08	8.11e-09
42×84	6.52e-06	5.45e-09	3.56e-10	9.47e-10	6.83e-11
48×96	1.25e-06	9.17e-10	9.18e-11	5.02e-11	5.72e-12
54×108	2.67e-07	5.11e-10	7.66e-11	6.11e-11	8.09e-12
60×120	7.60e-08	2.04e-10	9.00e-12	2.68e-11	5.90e-12

5.1.2. A cushion-shaped geometry. Next, the boundary is a cushion-shaped surface

$$(5.8) \quad \mathbf{r}(\theta, \phi) = \begin{bmatrix} f(\theta, \phi) \cos(\theta) \cos(\phi) \\ f(\theta, \phi) \sin(\theta) \cos(\phi) \\ f(\theta, \phi) \sin(\phi) \end{bmatrix}, \quad (\theta, \phi) \in [0, \pi] \times [0, 2\pi],$$

where the radial function is $f(\theta, \phi) = (4/5 + 1/2(\cos(2\theta) - 1)(\cos(4\phi) - 1))^{1/2}$. See the image on the left side of Figure 5.3. We use the ‘‘cubed sphere’’ in [60] to divide the cushion into six big charts, with each chart further divided into $2n_\theta \times n_\phi$ triangles. Thus, the total number of patches N_{patches} is $12n_\theta n_\phi$. Table 5.2 shows relative l_∞ error at sample data points of N_{patches} for $p = 4, 6, \dots, 14$. The image on the right side of Figure 5.3 plots the numerical convergence order with these data points and expected convergence order in dashed lines. Finally, Figure 5.4 show the pointwise relative errors at three orthogonal slices.

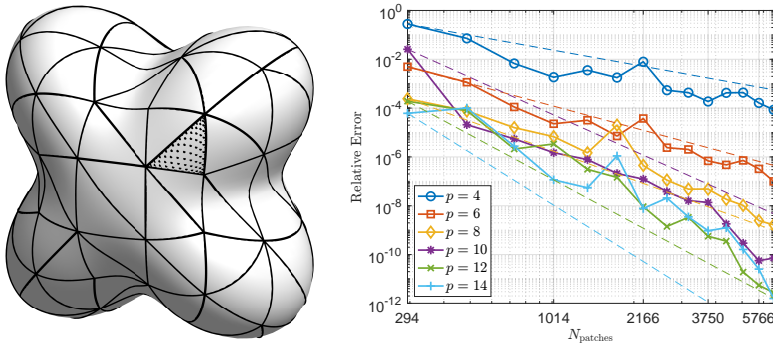


FIG. 5.3. Left: triangulated cushion-shaped boundary. Right: relative l_∞ errors as functions of N_{patches} for various orders p .

In both examples, we have used a more or less uniform triangulation in the parameter space. However, both geometries have some fine details that could be best resolved with some adaptivity employed in the triangulation. The somewhat noisy

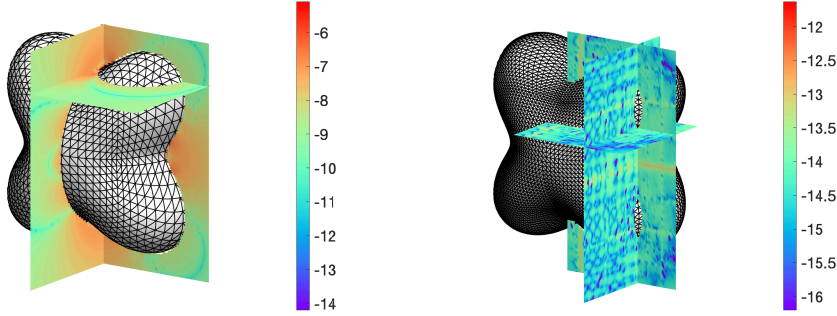


FIG. 5.4. Slice plots of \log_{10} of the pointwise relative errors for the cushion-shape boundary. Left: $p = 6, n_\theta = 17, n_\phi = 17$. Right: $p = 12, n_\theta = 33, n_\phi = 33$.

TABLE 5.2

Relative l_∞ errors E_∞ for the cushion shaped example at sample values of n_θ , n_ϕ , and p . The total number of patches is $N_{\text{patches}} = 12n_\theta n_\phi$ and the total number of discretization points is $N = N_{\text{patches}}p(p+1)/2$.

$12 \times n_\theta n_\phi$	p	6	8	10	12	14
12×9^2		9.75e-04	6.53e-05	2.16e-05	7.57e-05	8.25e-05
12×13^2		2.31e-05	6.11e-06	1.74e-06	3.60e-06	1.03e-07
12×17^2		8.76e-06	1.64e-05	1.74e-07	1.48e-07	1.22e-06
12×21^2		2.62e-06	1.32e-07	3.06e-08	1.26e-09	2.07e-08
12×25^2		6.17e-07	3.94e-08	1.19e-08	4.41e-10	8.74e-10
12×29^2		6.84e-07	9.26e-09	2.64e-10	1.54e-11	1.41e-10
12×33^2		1.21e-07	1.42e-09	6.22e-11	2.44e-12	1.44e-12

data points in the convergence plots are likely due to the under-resolved nonadaptive triangulation. We would also like to remark that most figures and tables in [79, 80] show the convergence for p up to 7 except Fig. 3, where values of p up to 10 are shown. While the original scheme in [79, 80] can achieve about ten digits of accuracy with adaptive integration for computing line integrals, our improved scheme achieves about twelve digits of accuracy.

5.2. Study of efficiency. Here, we demonstrate the efficiency of our quadrature scheme during the solve phase and the evaluation phase. For both cases, we use T_{FMM} as the benchmark to measure the relative throughput of our quadrature scheme in points processed per second per core.

5.2.1. Green's identity on a stellarator geometry. In the third example, we demonstrate the performance of our scheme by verifying the Green's identity

$$(5.9) \quad \frac{1}{2}u(\mathbf{r}') = \mathcal{S} \left[\frac{\partial u}{\partial n} \right] (\mathbf{r}') - \mathcal{D}[u](\mathbf{r}'), \quad \mathbf{r}' \in S.$$

The boundary is the surface of a typical stellarator

$$(5.10) \quad \mathbf{r}(u, v) = \sum_{i=-1}^2 \sum_{j=-1}^1 \delta_{i,j} \begin{bmatrix} \cos v \cos((1-i)u + jv) \\ \sin v \cos((1-i)u + jv) \\ \sin((1-i)u + jv) \end{bmatrix}, \quad (u, v) \in [0, 2\pi]^2,$$

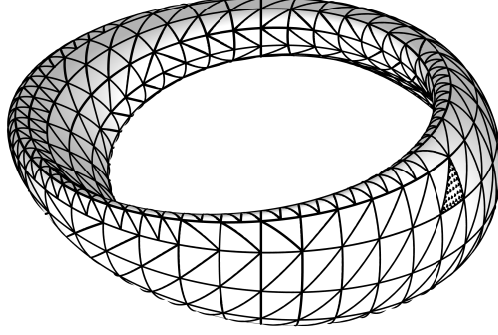


FIG. 5.5. Triangulated stellarator-shaped geometry.

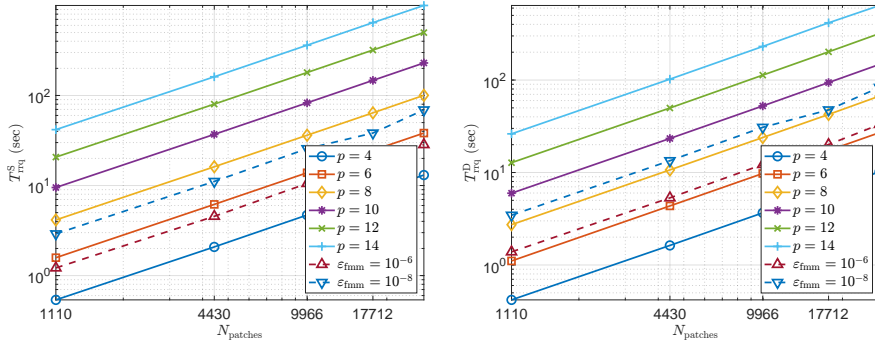


FIG. 5.6. Computation time in seconds in the quadrature correction part of Laplace layer potentials for the stellarator shaped boundary in Figure 5.5 for $p = 4, 6, \dots, 14$. Left: Computation time T_{RRQ} for the Laplace single layer potential operator. Right: Computation time T_{RRQ} for the Laplace double layer potential operator. In both figures, the dashed lines show the computation time on a single FMM call on the same set of points.

where the non-zero coefficients are $\delta_{-1,-1} = 0.17$, $\delta_{-1,0} = 0.11$, $\delta_{0,0} = 1$, $\delta_{1,0} = 4.5$, $\delta_{2,0} = -0.25$, $\delta_{0,1} = 0.07$, and $\delta_{2,1} = -0.45$. See the image on the left side of Figure 5.5. The triangulation is carried out by dividing the square in the parameter space into $n_u \times n_v$ equi-sized rectangles, with each rectangle further subdivided into two equal triangles. The stellarator has high curvature regions that rotate along one of the angular directions, introducing significant challenges for the accurate evaluation of layer potentials.

Figure 5.6 plots the computation time in the quadrature correction part of our scheme as a function of N_{patches} for the stellarator shaped boundary. Table 5.3 reports the throughput (in points processed per second per core) of our quadrature scheme. The first column lists the approximation order p . The second column lists the throughput of our quadrature scheme for the Laplace single layer potential operator, i.e.,

$$(5.11) \quad X_{RRQ}^S = N/T_{RRQ}^S,$$

where N is the total number of discretization points on the boundary and T_{RRQ}^S is the time for building the sparse quadrature correction matrix for the SLP. The third column lists the throughput of a single FMM call for evaluating the smooth part of

TABLE 5.3

Throughput in points processed per second per core of our quadrature scheme during the solve phase for the stellarator shaped boundary.

p	X_{RRQ}^S	X_{FMM}^S	X_{RRQ}^D	X_{FMM}^D	ε_{FMM}	E_∞
4	21285	26894	27212	24144	1.00e-04	1.08e-04
6	15065	20445	21376	17494	1.00e-06	2.07e-05
8	9921	13983	15017	11646	1.00e-08	2.76e-07
10	6621	13341	10449	10803	1.00e-09	3.15e-08
12	4324	9888	6845	8089	1.00e-10	7.59e-10
14	2907	9113	4534	7178	1.00e-12	9.74e-12

the SLP, i.e.,

$$(5.12) \quad X_{\text{FMM}}^S = N/T_{\text{FMM}}^S,$$

where T_{FMM}^S is the time on applying $\mathbf{S}_{\text{smooth}}$ to a given vector using the FMM. The fourth column lists the throughput of our quadrature scheme for the Laplace double layer potential operator. The fifth column lists the throughput of a single FMM call for evaluating the smooth part of the DLP. The sixth column lists the tolerance used in the FMM. And the last column lists the relative l_∞ error for verifying Green's identity in (5.9).

We would like to compare this table with the previous state-of-the-art optimized adaptive quadrature scheme in [32]. In [32, Table 1(c), (d)], the speeds for p up to 8 are reported. At about six digits of accuracy, the throughput for $p = 8$ for the Helmholtz single layer potential in [32] is 945 points per second per core, the throughput for the Helmholtz FMM is about 5960 points per second per core. That is, the throughput in the quadrature correction is approximately six times slower than the FMM. On the other hand, the throughput in the quadrature correction of our scheme is 9921 per second per core for the Laplace single layer potential operator and 15017 per second per core for the Laplace double layer potential operator, both of which are close to the FMM speed. Note that if iterative solvers such as GMRES are used to solve the resulting linear system, then the sparse matrices \mathbf{S}_{RRQ} and \mathbf{D}_{RRQ} only need to be built once, while the FMM has to be applied N_{iter} times. Here, N_{iter} is the number of GMRES iterations to reach the prescribed tolerance, which ranges from 10 to low hundreds for well-conditioned problems, but could be much larger for ill-conditioned problems.

REMARK 5.1. *Although we use the FMM as a benchmark to demonstrate the performance of our quadrature scheme, its efficiency is also quite important for fast direct solvers [6, 13, 16, 24, 31, 42, 44, 43, 46, 49, 50, 51, 53, 73]. In these solvers, generating matrix entries for discretized integral operators consumes a significant amount of time when constructing sparse representations of the system matrix and its inverse.*

5.2.2. Interlocking tori. Next, we assess the performance of our quadrature scheme during the evaluation phase, where layer potentials are evaluated in a volumetric grid. That is, N_S sources are on the boundary and N_T targets are in the entire computational domain with $N_T \gg N_S$. Such tasks are often encountered when the solution to the PDE in the whole volume is required, or when the PDE has an inhomogeneous term, i.e., the governing equation is the Poisson equation instead of the Laplace equation (see, for example, [21]). We set up a complex geometry test example where the predominant cost of layer potential evaluation comes from computing

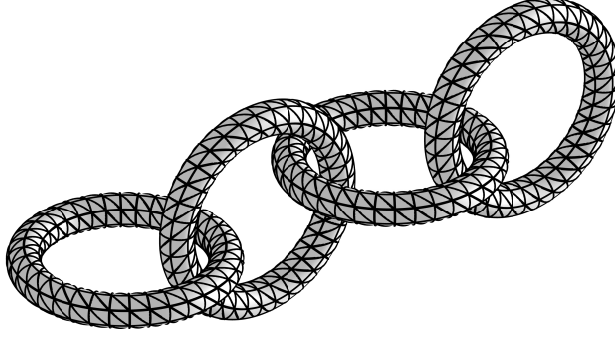


FIG. 5.7. Boundary with four interlocking tori.

nearly singular integrals. The boundary consists of four interlocking tori, where each torus is a shifted and rotated version of (5.7), with parameters $a = 3$, $b = 0.5$, $\omega_c = 0$, $\omega_n = 0$ and $\omega_m = 0$. A translation of 4.95 along the x -direction is applied so that the shortest distance between two adjacent tori is 0.05. See Figure 5.7.

Each torus surface is discretized into four different configurations: 6×36 , 12×72 , 18×108 , and 24×144 rectangles, with each rectangle further subdivided into two equal triangular patches in the parameter space. For each discretization, we solve the exterior Dirichlet problem (5.2), then evaluate the solution u on a corresponding uniform grid of $101 \times 101 \times 101$, $201 \times 201 \times 201$, $301 \times 301 \times 301$, and $401 \times 401 \times 401$ points within the bounding box $[-5, 20] \times [-6, 6] \times [-6, 6]$ enclosing the boundary. The total number of target points in the exterior of the interlocking tori is $N_T = [1013571, 7988041, 26825787, 63428399]$ for these four cases, out of which there are $N_T^c = [328492, 1198758, 2627046, 4613672]$ close target points that require quadrature correction, respectively.

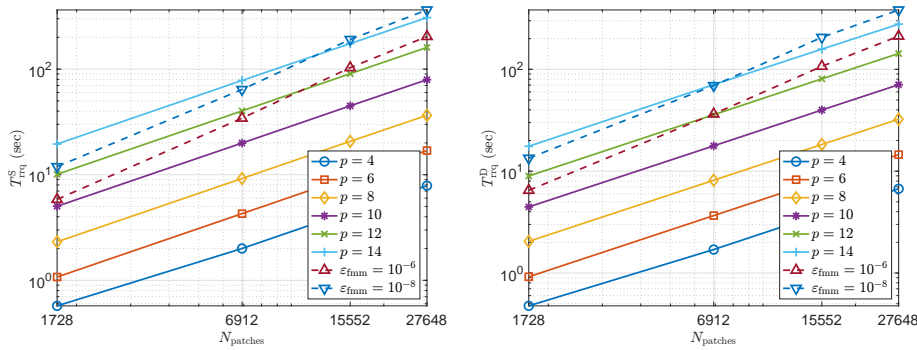


FIG. 5.8. Computation time in seconds in the quadrature correction part for the volumetric evaluation of Laplace layer potentials for the interlocking-tori boundary in Figure 5.7 for $p = 4, 6, \dots, 14$. Left: Computation time T_{RRQ}^S for the Laplace single layer potential operator. Right: Computation time T_{RRQ}^D for the Laplace double layer potential operator. In both figures, the dashed lines show the computation time on a single FMM call on the same set of source points on the boundary and target points in the volume.

Figure 5.8 plots the computation time in the quadrature correction part of our scheme as a function of N_{patches} for the interlocking-tori boundary. Table 5.4 reports the throughput (in points processed per second per core) of our quadrature scheme

when layer potentials are viewed as maps from the boundary to the volume. Here the throughput for the quadrature correction part is defined via the formulas

$$(5.13) \quad X_{\text{RRQ}}^S = N_T^c / T_{\text{RRQ}}^S, \quad X_{\text{RRQ}}^D = N_T^c / T_{\text{RRQ}}^D,$$

and the throughput for the FMM part is defined via the formulas

$$(5.14) \quad X_{\text{FMM}}^S = N_T / T_{\text{FMM}}^S, \quad X_{\text{FMM}}^D = N_T / T_{\text{FMM}}^D.$$

Note that N_T^c is a small fraction of N_T . Thus, the time spent on quadrature correction is a small fraction of that on the FMM, even though the throughput are close to each other.

TABLE 5.4

Throughput in points processed per second per core of our quadrature scheme during the evaluation phase for the interlock-tori boundary.

p	X_{RRQ}^S	X_{FMM}^S	X_{RRQ}^D	X_{FMM}^D	ε_{FMM}	E_∞
4	583929	468224	687077	433446	1.00e-04	1.14e-04
6	272680	260129	318736	250650	1.00e-06	1.41e-06
8	126596	140465	143307	130197	1.00e-08	3.22e-08
10	58368	108913	65770	102488	1.00e-09	7.47e-10
12	28941	74238	32493	69085	1.00e-10	1.33e-11
14	14995	55063	16584	50249	1.00e-12	6.11e-12

6. Conclusions and further discussions. We have developed a recursive reduction quadrature (RRQ) scheme for evaluating Laplace layer potentials on surfaces in three dimensions. The RRQ scheme starts from a quaternion harmonic polynomial approximation of the density for the Laplace double layer potential. Since harmonic polynomials are defined over the entire ambient space, this approximation naturally extends to a small volumetric neighborhood of the surface patch. Moreover, the quaternion harmonic polynomial approximation is constructed so that the general Stokes theorem can be applied to reduce the surface integrals to line integrals over the boundary of the patch. Certain degrees of freedom exist in choosing these line integrals, and we have adopted target-centered formulas to derive these 1-forms. The resulting line integrals have exactly the same singularities as the kernels in the original surface integrals. We then apply singularity-swap quadrature to evaluate these line integrals recursively. In other words, line integrals are evaluated via integration by parts, this time by extending the real parameter of the boundary curve into the complex plane. Altogether, we have been able to reduce the evaluation of singular and nearly singular surface integrals to function evaluations at the vertices of the triangular patch. The resulting scheme can handle self and near interactions, as well as close evaluations, with unparalleled accuracy and efficiency.

As observed in [79, 80], the closest relative of our quadrature scheme is the *kernel-split quadrature* developed by Johan Helsing and his collaborators [35, 36, 37, 38, 39, 40, 41], which has been extended to evaluating almost all layer potentials in two dimensions. Indeed, extending RRQ to other layer potentials in three dimensions, such as the Helmholtz, Stokes, and elastic layer potentials, is straightforward. Moreover, the recursive reduction approach used in our quadrature construction is independent of the shapes of patches and can thus be easily extended to, for example, quadrilateral patches. We are currently working on these extensions, and the findings will be reported at a later date.

7. Acknowledgments. The authors would like to thank Charles Epstein and Leslie Greengard for helpful discussions.

REFERENCES

- [1] L. AF KLINTEBERG AND A. H. BARNETT, *Accurate quadrature of nearly singular line integrals in two and three dimensions by singularity swapping*, BIT Numerical Mathematics, 61 (2021), pp. 83–118.
- [2] J. S. ASVESTAS, *Line integrals and physical optics. Part I. The transformation of the solid-angle surface integral to a line integral*, J. Opt. Soc. Am. A, 2 (1985), pp. 891–895.
- [3] ———, *Line integrals and physical optics. Part II. The conversion of the Kirchhoff surface integral to a line integral*, J. Opt. Soc. Am. A, 2 (1985), pp. 896–902.
- [4] J. T. BEALE, *A grid-based boundary integral method for elliptic problems in three dimensions*, SIAM Journal on Numerical Analysis, 42 (2004), pp. 599–620.
- [5] J. T. BEALE AND S. TLUPOVA, *Extrapolated regularization of nearly singular integrals on surfaces*, Advances in Computational Mathematics, 50 (2024), p. 61.
- [6] J. BREMER, *A fast direct solver for the integral equations of scattering theory on planar curves with corners*, J. Comput. Phys., 231 (2012), pp. 1879–1899.
- [7] J. BREMER AND Z. GIMBUTAS, *A Nyström method for weakly singular integral operators on surfaces*, J. Comput. Phys., 231 (2012), pp. 4885–4903.
- [8] ———, *On the numerical evaluation of the singular integrals of scattering theory*, J. Comput. Phys., 251 (2013), pp. 327–343.
- [9] J. BREMER, Z. GIMBUTAS, AND V. ROKHLIN, *A nonlinear optimization procedure for generalized Gaussian quadratures*, SIAM J. Sci. Comput., 32 (2010), pp. 1761–1788.
- [10] O. P. BRUNO AND L. A. KUNYANSKY, *A fast, high-order algorithm for the solution of surface scattering problems: basic implementation, tests, and applications*, J. Comput. Phys., 169 (2001), pp. 80–110.
- [11] ———, *Surface scattering in three dimensions: an accelerated high-order solver*, R. Soc. Lond. Proc. Ser. A Math. Phys. Eng. Sci., 457 (2001), pp. 2921–2934.
- [12] J. CARRIER, L. GREENGARD, AND V. ROKHLIN, *A fast adaptive multipole algorithm for particle simulations*, SIAM J. Sci. Statist. Comput., 9 (1988), pp. 669–686.
- [13] S. CHANDRASEKARAN, M. GU, AND T. PALS, *A fast ULV decomposition solver for hierarchically semiseparable representations*, SIAM J. Matrix Anal. Appl., 28 (2006), pp. 603–622.
- [14] H. CHENG, L. GREENGARD, AND V. ROKHLIN, *A fast adaptive multipole algorithm in three dimensions*, J. Comput. Phys., 155 (1999), pp. 468–498.
- [15] D. COLTON AND R. KRESS, *Inverse acoustic and electromagnetic scattering theory*, vol. 93 of Applied Mathematical Sciences, Springer-Verlag, Berlin, second ed., 1998.
- [16] E. CORONA, P.-G. MARTINSSON, AND D. ZORIN, *An $O(N)$ direct solver for integral equations on the plane*, Appl. Comput. Harmon. Anal., 38 (2015), pp. 284–317.
- [17] L. DING, J. HUANG, J. L. MARZUOLA, AND Z. TANG, *Quadrature by two expansions: Evaluating laplace layer potentials using complex polynomial and plane wave expansions*, Journal of Computational Physics, 428 (2021), p. 109963.
- [18] M. P. DO CARMO, *Differential forms and applications*, Springer, 1998.
- [19] R. DUAN AND V. ROKHLIN, *High-order quadratures for the solution of scattering problems in two dimensions*, Journal of Computational Physics, 228 (2009), pp. 2152–2174.
- [20] M. G. DUFFY, *Quadrature over a pyramid or cube of integrands with a singularity at a vertex*, SIAM J. Numer. Anal., 19 (1982), pp. 1260–1262.
- [21] C. L. EPSTEIN, F. FRYKLUND, AND S. JIANG, *An accurate and efficient scheme for function extensions on smooth domains*, revised 2023.
- [22] C. L. EPSTEIN, L. GREENGARD, AND A. KLÖCKNER, *On the Convergence of Local Expansions of Layer Potentials*, SIAM J. Numer. Anal., 51 (2013), pp. 2660–2679.
- [23] W. FONG AND E. DARVE, *The black-box fast multipole method*, J. Comput. Phys., 228 (2009), pp. 8712–8725.
- [24] A. GILLMAN, P. M. YOUNG, AND P.-G. MARTINSSON, *A direct solver with $O(N)$ complexity for integral equations on one-dimensional domains*, Front. Math. China, 7 (2012), pp. 217–247.
- [25] Z. GIMBTUAS, L. GREENGARD, L. LU, J. MAGLAND, D. MALHOTRA, M. O’NEIL, M. RACHH, AND V. ROKHLIN, *Flatiron Institute Fast Multipole Libraries*. <https://github.com/flatironinstitute/FMM3D>, 2020.
- [26] Z. GIMBUTAS AND V. ROKHLIN, *A generalized fast multipole method for nonoscillatory kernels*, SIAM J. Sci. Comput., 24 (2002), pp. 796–817.
- [27] Z. GIMBUTAS AND S. VEERAPANENI, *A fast algorithm for spherical grid rotations and its applica-*

- tion to singular quadrature, *SIAM Journal on Scientific Computing*, 35 (2013), pp. A2738–A2751.
- [28] I. G. GRAHAM AND I. H. SLOAN, *Fully discrete spectral boundary integral methods for helmholtz problems on smooth closed surfaces in \mathbb{R}^3* , *Numerische Mathematik*, 92 (2002), pp. 289–323.
- [29] L. GREENGARD, *Rapid evaluation of potential fields in particle systems*, PhD thesis, Yale University, New Haven, CT (USA), 1987.
- [30] L. GREENGARD, *The rapid evaluation of potential fields in particle systems*, MIT press, 1988.
- [31] L. GREENGARD, D. GUEYFFIER, P.-G. MARTINSSON, AND V. ROKHLIN, *Fast direct solvers for integral equations in complex three-dimensional domains*, *Acta Numer.*, 18 (2009), pp. 243–275.
- [32] L. GREENGARD, M. O’NEIL, M. RACHH, AND F. VICO, *Fast multipole methods for the evaluation of layer potentials with locally-corrected quadratures*, *Journal of Computational Physics*: X, 10 (2021), p. 100092.
- [33] L. GREENGARD AND V. ROKHLIN, *A fast algorithm for particle simulations*, *J. Comput. Phys.*, 73 (1987), pp. 325–348.
- [34] ———, *A new version of the fast multipole method for the Laplace equation in three dimensions*, in *Acta numerica*, 1997, vol. 6 of *Acta Numer.*, Cambridge Univ. Press, 1997, pp. 229–269.
- [35] J. HELSING, *A fast and stable solver for singular integral equations on piecewise smooth curves*, *SIAM J. Sci. Comput.*, 33 (2011), pp. 153–174.
- [36] J. HELSING AND A. HOLST, *Variants of an explicit kernel-split panel-based nyström discretization scheme for helmholtz boundary value problems*, *Advances in Computational Mathematics*, 41 (2015), pp. 691–708.
- [37] J. HELSING AND S. JIANG, *On integral equation methods for the first dirichlet problem of the biharmonic and modified biharmonic equations in nonsmooth domains*, *SIAM Journal on Scientific Computing*, 40 (2018), pp. A2609–A2630.
- [38] J. HELSING AND A. KARLSSON, *An explicit kernel-split panel-based Nyström scheme for integral equations on axially symmetric surfaces*, *Journal of Computational Physics*, 272 (2014), pp. 686–703.
- [39] ———, *On a Helmholtz transmission problem in planar domains with corners*, *Journal of Computational Physics*, 371 (2018), pp. 315–332.
- [40] J. HELSING AND R. OJALA, *Corner singularities for elliptic problems: Integral equations, graded meshes, quadrature, and compressed inverse preconditioning*, *Journal of Computational Physics*, 227 (2008), pp. 8820–8840.
- [41] ———, *On the evaluation of layer potentials close to their sources*, *Journal of Computational Physics*, 227 (2008), pp. 2899–2921.
- [42] K. L. HO AND L. GREENGARD, *A fast direct solver for structured linear systems by recursive skeletonization*, *SIAM J. Sci. Comput.*, 34 (2012), pp. A2507–A2532.
- [43] K. L. HO AND L. YING, *Hierarchical interpolative factorization for elliptic operators: differential equations*, *Comm. Pure Appl. Math.*, 69 (2016), pp. 1415–1451.
- [44] ———, *Hierarchical interpolative factorization for elliptic operators: integral equations*, *Comm. Pure Appl. Math.*, 69 (2016), pp. 1314–1353.
- [45] A. KLOECKNER, A. BARNETT, L. GREENGARD, AND M. O’NEIL, *Quadrature by expansion: A new method for the evaluation of layer potentials*, *J. Comput. Phys.*, 252 (2013), pp. 332–349.
- [46] W. Y. KONG, J. BREMER, AND V. ROKHLIN, *An adaptive fast direct solver for boundary integral equations in two dimensions*, *Appl. Comput. Harmon. Anal.*, 31 (2011), pp. 346–369.
- [47] T. KOORNWINDER, *Two-variable analogues of the classical orthogonal polynomials*, in *Theory and application of special functions*, Elsevier, 1975, pp. 435–495.
- [48] J. MA, V. ROKHLIN, AND S. WANDZURA, *Generalized Gaussian quadrature rules for systems of arbitrary functions*, *SIAM J. Numer. Anal.*, 33 (1996), pp. 971–996.
- [49] P. G. MARTINSSON, *A fast direct solver for a class of elliptic partial differential equations*, *J. Sci. Comput.*, 38 (2009), pp. 316–330.
- [50] P. G. MARTINSSON AND V. ROKHLIN, *A fast direct solver for boundary integral equations in two dimensions*, *J. Comput. Phys.*, 205 (2005), pp. 1–23.
- [51] ———, *A fast direct solver for scattering problems involving elongated structures*, *J. Comput. Phys.*, 221 (2007), pp. 288–302.
- [52] A. V. MASKET, *Solid angle contour integrals, series, and tables*, *Review of Scientific Instruments*, 28 (1957), pp. 191–197.
- [53] V. MINDEN, K. L. HO, A. DAMLE, AND L. YING., *A recursive skeletonization factorization based on strong admissibility*, *SIAM Multiscale Model. Simul.*, 69 (2017), pp. 1415–1451.
- [54] M. J. MORSE, A. RAHIMIAN, AND D. ZORIN, *A robust solver for elliptic pdes in 3d complex*

- geometries*, Journal of Computational Physics, 442 (2021), p. 110511.
- [55] F. W. J. OLVER, D. W. LOZIER, R. F. BOISVERT, AND C. W. CLARK, eds., *NIST Handbook of Mathematical Functions*, Cambridge University Press, May 2010.
- [56] C. PÉREZ-ARANCIBIA, L. M. FARIA, AND C. TURC, *Harmonic density interpolation methods for high-order evaluation of laplace layer potentials in 2d and 3d*, Journal of Computational Physics, 376 (2019), pp. 411–434.
- [57] C. PÉREZ-ARANCIBIA, C. TURC, AND L. FARIA, *Planewave density interpolation methods for 3d helmholtz boundary integral equations*, SIAM Journal on Scientific Computing, 41 (2019), pp. A2088–A2116.
- [58] M. RACHH ET AL., *FMM-accelerated boundary integral equation solvers*. <https://github.com/fastalgorithms/fmm3dbie>, 2024.
- [59] M. RACHH, A. KLÖCKNER, AND M. O’NEIL, *Fast algorithms for quadrature by expansion i: Globally valid expansions*, Journal of Computational Physics, 345 (2017), pp. 706–731.
- [60] C. RONCHI, R. IACONO, AND P. S. PAOLUCCI, *The “cubed sphere”: A new method for the solution of partial differential equations in spherical geometry*, Journal of computational physics, 124 (1996), pp. 93–114.
- [61] A. ROSÉN, *Geometric multivector analysis*, Springer, 2019.
- [62] Y. SAAD AND M. H. SCHULTZ, *GMRES: a generalized minimal residual algorithm for solving nonsymmetric linear systems*, SIAM J. Sci. Statist. Comput., 7 (1986), pp. 856–869.
- [63] R. SAYE, *High-order methods for computing distances to implicitly defined surfaces*, Communications in Applied Mathematics and Computational Science, 9 (2014), pp. 107–141.
- [64] M. SIEGEL AND A.-K. TORNBORG, *A local target specific quadrature by expansion method for evaluation of layer potentials in 3d*, Journal of Computational Physics, 364 (2018), pp. 365–392.
- [65] D. B. STEIN AND A. H. BARNETT, *Quadrature by fundamental solutions: kernel-independent layer potential evaluation for large collections of simple objects*, Advances in Computational Mathematics, 48 (2022), p. 60.
- [66] H. SUNDAR, R. S. SAMPATH, AND G. BIROS, *Bottom-up construction and 2 : 1 balance refinement of linear octrees in parallel*, SIAM J. Sci. Comput., 30 (2008), pp. 2675–2708.
- [67] B. VIOREANU AND V. ROKHLIN, *Spectra of multiplication operators as a numerical tool*, SIAM J. Sci. Comput., 36 (2014), pp. A267–A288.
- [68] M. WALA AND A. KLÖCKNER, *A fast algorithm for quadrature by expansion in three dimensions*, Journal of Computational Physics, 388 (2019), pp. 655–689.
- [69] ———, *Optimization of fast algorithms for global quadrature by expansion using target-specific expansions*, Journal of Computational Physics, 403 (2020), p. 108976.
- [70] B. WU AND P.-G. MARTINSSON, *Corrected trapezoidal rules for boundary integral equations in three dimensions*, Numerische Mathematik, 149 (2021), pp. 1025–1071.
- [71] ———, *Zeta correction: a new approach to constructing corrected trapezoidal quadrature rules for singular integral operators*, Advances in Computational Mathematics, 47 (2021), p. 45.
- [72] ———, *A unified trapezoidal quadrature method for singular and hypersingular boundary integral operators on curved surfaces*, SIAM Journal on Numerical Analysis, 61 (2023), pp. 2182–2208.
- [73] J. XIA, S. CHANDRASEKARAN, M. GU, AND X. LI, *Fast algorithms for hierarchically semiseparable matrices*, Numer. Linear Algebra Appl., 17 (2010), pp. 953–976.
- [74] H. XIAO AND Z. GIMBUTAS, *A numerical algorithm for the construction of efficient quadrature rules in two and higher dimensions*, Comput. Math. Appl., 59 (2010), pp. 663–676.
- [75] N. YARVIN AND V. ROKHLIN, *Generalized Gaussian quadratures and singular value decompositions of integral operators*, SIAM J. Sci. Comput., 20 (1998), pp. 699–718.
- [76] L. YING, G. BIROS, AND D. ZORIN, *A kernel-independent adaptive fast multipole algorithm in two and three dimensions*, J. Comput. Phys., 196 (2004), pp. 591–626.
- [77] C. D. YU, J. HUANG, W. AUSTIN, B. XIAO, AND G. BIROS, *Performance optimization for the k-nearest neighbors kernel on x86 architectures*, in Proceedings of the International Conference for High Performance Computing, Networking, Storage and Analysis, 2015, pp. 1–12.
- [78] B. ZHANG, J. HUANG, N. P. PITSIANIS, AND X. SUN, *A Fourier-series-based kernel-independent fast multipole method*, J. Comput. Phys., 230 (2011), pp. 5807–5821.
- [79] H. ZHU, *Fast, High-Order Accurate Integral Equation Methods and Application to PDE-Constrained Optimization*, PhD thesis, University of Michigan, Ann Arbor, MI (USA), 2021.
- [80] H. ZHU AND S. VEERAPANENI, *High-order close evaluation of Laplace layer potentials: A differential geometric approach*, SIAM Journal on Scientific Computing, 44 (2022), pp. A1381–A1404.